Optimal frequency band selection using blind and targeted features for spectral coherence-based bearing diagnostics: A comparative study

Abstract

Identifying a spectral frequency band with abundant fault information from spectral coherence is essential for improved envelope spectrum-based bearing diagnosis. Both blind features and targeted features have been employed to distinguish informative spectral frequency band of spectral coherence. However, how to select appropriate feature to correctly discriminate the optimal frequency band of spectral coherence in different scenarios is problematic. In this study, a new targeted feature is presented to quantify the signal-to-noise ratio in narrow frequency bands of spectral coherence, and further a method based on the proposed feature is developed to distinguish an optimal spectral frequency band of spectral coherence for bearing diagnostics. The efficiency of the developed method, typical blind feature-based methods and typical targeted feature-based methods in identifying the defect-sensitive frequency band of spectral coherence and bearing fault diagnosis is validated and compared using simulated signals with different interference noises and bearing experimental signals. The advantages and limitations of typical blind and targeted feature-based methods in different scenarios are summarized to guide the application. The results demonstrate that the developed targeted feature can efficiently evaluate bearing failure information in the cyclic frequency domain, and the presented approach can accurately discriminate the failure-related spectral frequency band of spectral coherence and detect different bearing faults compared with the methods based on the state-of-the-art features.

Keywords: Improved envelope spectrum; sparsity measures; targeted features; spectral coherence; bearing diagnostics

1. Introduction

Modern mechanical systems widely adopt rolling bearings to support rotating shafts or rotors to reduce friction. Harsh service conditions, such as high speed, large load, and multiple interferences, make rolling bearings one of the parts that are prone to malfunction in rotating machinery systems [1–3]. Therefore, bearing fault diagnostics and prognostics are critical to ensure the safe operation of mechanical systems and have attracted increasing attention in recent years [4].

Squared Envelope Spectrum (SES) analysis conducted on the band-pass filtering signal with rich fault information is a commonly used signal processing technique for bearing failure diagnostics. The central issue of envelope analysis technique is to distinguish an informative spectral frequency band (ISFB) to recover the repeated transient impulses caused by localized bearing defects. The representative methods are the fast Kurtogram [5] and the Protrugram [6]. The former uses a filter bank in the form of a 1/3-binary tree to decompose the entire spectral frequency band into sub-bands with different bandwidths and center frequencies and takes the kurtosis of narrow-band filtered signal (characterizing impulsiveness) as the criterion for selecting ISFB, while the latter adopts the kurtosis of the envelope spectrum of the filtered signal in a narrow band split by a sliding window along the frequency axis as a feature (characterizing cyclostationarity) to identify ISFB. Later, Antoni [7] used negentropy (NE) to incorporate the cyclostationarity and impulsiveness of bearing fault signals into Infogram to discriminate ISFB. Tse and Wang [8] employed the ratio of L2 norm to L1 norm (L2/L1) to distinguish the ISFB for bearing fault detection. The effectiveness of similar features, including

Nomenclature	
BPFI	Ball Pass Frequency of Inner Race
BPFO	Ball Pass Frequency of Outer Race
DF	Diagnostic Feature
EES	Enhanced Envelope Spectrum
FDSNR	Frequency Domain Signal-to-Noise Ratio
GI	Gini Index
HI	Hoyer Index
IES	Improved Envelope Spectrum
IESFOgram	Improved Envelope Spectrum via Feature Optimization-gram
ISFB	Informative Spectral Frequency Band
ICS2	Indicator of Second-order Cyclostationarity
Kurt	Kurtosis
L2/L1	Ratio of L2 norm to L1 norm
NE	Negentropy
RCC	Ratio of Cyclic Content
RSI	Reciprocal of Smoothness Index
SC	Spectral Correlation
SCoh	Spectral Coherence
SD	Spectral Density
SES	Squared Envelope Spectrum
SNR	Signal-to-Noise Ratio

Hoyer index (HI) [9], the reciprocal of smoothness index (RSI) [10], Gini index (GI) [11], stability index and conditional variance statistic [12], in detecting and quantifying fault information contained in narrowband signals has been investigated in [13–15]. These features do not require prior knowledge of mechanical faults and can be called blind features. In the last few years, increasing attention has been shifted to the cyclostationarity of bearing fault symptoms, and some band selection tools have been developed by establishing the indicators of characterizing cyclostationarity, including indicator of second-order cyclostationarity (ICS2) [16], the ratio of cyclic content (RCC) [17], cyclic harmonic ratio [18], distcsgram [19] and the log-cycligram [20]. These features require prior knowledge from the fault characteristic frequency or signal distribution hypothesis and can be called the targeted features.

The bearing fault signals have been demonstrated to be second-order cyclostationary, and the well-established analytical tools are Spectral Correlation (SC) as well as its normalized form, namely Spectral Coherence (SCoh) [21,22]. The SC and SCoh are dual-frequency representations and can simultaneously reveal the resonance frequency bands and characteristic frequencies induced by bearing defects. The Enhanced Envelope Spectrum (EES) obtained by the integration of the SCoh over the entire spectral frequency range has shown more effective performance in revealing the fault-related cyclostationary features than traditional SES [23]. Since EES carries the information contained in the entire spectral frequency band, complex interference noise can easily distort EES, making it difficult to distinguish characteristic frequencies relevant to bearing defects. Improved Envelope Spectrum (IES) [21,23] obtained by integrating the SCoh over an ISFB is an effective solution to reduce complex interference noise and enhance fault-related cyclic components. Thus, how to determine a spectral frequency band containing diagnostic information from SCoh to generate IES is the key to accurately

identifying bearing faults.

A blind approach was developed to determine the ISFBs for the IES-based bearing fault diagnosis in [24]. This method employs the L2/L1 norm of the IES obtained by the integration of SCoh over a narrow spectral frequency range as the band selection criterion. Similarly, the kurtosis enhanced spectral entropy was proposed to determine the ISFBs from the entire spectral frequency range of SCoh for constructing fault-sensitive IESs in [25]. However, these methods primarily count on visual inspection rather than adaptive mechanisms to identify ISFBs. Mauricio et al. [26,27] proposed an adaptive method to select an ISFB for the IES-based rotating machinery diagnostics, namely Improved Envelope Spectrum via Feature Optimization-gram (IESFOgram). In this method, the entire spectral frequency band is divided into a 1/3-binary tree form to generate a group of narrow bands with different bandwidths and center frequencies, and then a targeted feature estimated from the IES obtained by integrating the SCoh over the divided band is optimized to determine a fault-sensitive ISFB. The IESFOgram has been applied to the gearbox bearing diagnostics under electromagnetic interferences [26,28–31] and time-varying operating conditions [27,32]. Similarly, a signal-to-noise ratio (SNR) measure was proposed by Schmidt et al. [33] to identify an ISFB of SCoh for gearbox fault diagnosis. These methods mainly rely on the sensitivity of blind or targeted features to fault components to identify ISFB, which greatly expand and enrich the application of SCoh in bearing fault identification. However, how to select appropriate criteria to correctly discriminate the ISFB to generate fault-sensitive IES in different application scenarios is problematic. Thus, it is very important to systematically investigate and compare the performances of different features in identifying ISFB to guide the applications of SCoh in bearing fault diagnosis.

To effectively evaluate the fault information contained in the narrow bands of SCoh, a novel targeted feature defined in the cyclic frequency domain is presented in this study. Further, the performance of the proposed feature and state-of-the-art features in identifying ISFB of SCoh and detecting bearing faults is validated and compared using simulated and experimental signals. To sum up, the contributions and innovations of this study mainly include:

(1) A novel feature indicator aimed at measuring the SNR in the cyclic frequency domain is proposed to evaluate the bearing fault information. Further, a method combining the 1/3-binary tree frequency band division technology and the proposed feature is developed to identify the optimal ISFB of SCoh for bearing fault diagnosis.

(2) Simulation analysis and experimental analysis are conducted to testify and compare the efficiency of the presented approach and the methods based on typical blind and targeted features in selecting ISFB of SCoh and bearing diagnostics, and the advantages and limitations of typical blind and targeted feature-based methods in different application scenarios are summarized.

(3) The performance of the presented approach and the methods based on typical blind and targeted features are qualitatively and quantitatively compared, and the results indicate that the presented approach can more efficiently distinguish a failure-related frequency band of SCoh and detect bearing faults under different interference noises in contrast to the methods based on typical blind and targeted features.

The remnants of this article are arranged as follows. Section 2 reviews the essential theories of the SCoh, IES and IESFOgram. In Section 3, typical blind and targeted features that disclose the cyclostationarity of bearing failure symptoms are discussed and the developed targeted feature is introduced. In Section 4, the comparison analysis of fault detection performance of the proposed method and typical blind and targeted feature-based methods is conducted on different simulated

signals. Section 5 presents the fault detection results of the proposed method and typical blind and targeted feature-based methods on different bearing experimental signals. In Section 6, the important conclusions are summarized.

2. Theoretical background

2.1. Spectral Coherence and Improved Envelope Spectrum

Let $x(t_n)$ be a bearing vibration signal, $t_n = n/F_s, n = 0,1,\cdots,N-1$, where F_s and N are the sampling rate and length, respectively. Assume that the bearing vibration signal $x(t_n)$ is second-order cyclostationary, its instantaneous autocorrelation function is defined by [23]:

$$R_x(t_n,\tau_m) = E\left\{x(t_n)x^*(t_n-\tau_m)\right\} \tag{1}$$

where $E\{\cdot\}$ indicates the ensemble mean operator, $*$ the complex conjugate, and $\tau_m = m/F_s$. The SC is ruled as the two-dimensional discrete Fourier transform of $R_x(t_n,\tau_m)$ [23]:

$$S_x(\alpha,f) = \lim_{N\to\infty}\frac{1}{(2N+1)F_s}\sum_{n=-N}^{N}\sum_{m=-\infty}^{\infty}R_x(t_n,\tau_m)e^{-j2\pi n\frac{\alpha}{F_s}}e^{-j2\pi m\frac{f}{F_s}} \tag{2}$$

Some estimation algorithms of the SC have been developed for practical applications [23,34–36]. Among them, the fast SC algorithm [23] achieves a significant reduction in computational burden and is therefore employed to calculate the SC in this work. The normalized form of the SC, namely the SCoh, is often used to enhance weak cyclostationary components, as follows [22]:

$$\gamma_x(\alpha,f) = \frac{S_x(\alpha,f)}{\sqrt{S_x(0,f)S_x(0,f-\alpha)}} \tag{3}$$

Integrating the SCoh along the spectral frequency axis, a one-dimensional spectrum quantity, namely the EES, can be constructed as [23]:

$$\mathrm{EES}(\alpha) = \frac{1}{F_s/2}\int_0^{F_s/2}\left|\gamma_x(\alpha,f)\right|df \tag{4}$$

The EES has shown better performance than the SES in bearing diagnostics [23]. However, since EES carries the information contained in the entire spectral frequency band, complex interference noise can easily cause distortion of EES, making it difficult to distinguish the defect-relevant frequencies. Thus, the IES generated from SCoh in an ISFB is recommended for bearing fault diagnosis [21,23]:

$$\mathrm{IES}(\alpha) = \frac{1}{f_2-f_1}\int_{f_1}^{f_2}\left|\gamma_x(\alpha,f)\right|df \tag{5}$$

where f_1 and f_2 denote the starting and ending frequencies of the selected spectral frequency band, respectively.

The band selection has a crucial influence on the fault detection performance because the characteristic frequency of interest can hardly be detected from the IES if the spectral frequency band is incorrectly selected. Thus, how to identify a spectral frequency band containing diagnostic information from SCoh to generate IES is the key to accurately detecting bearing faults.

2.2. Improved Envelope Spectrum via Feature Optimization-gram

IESFOgram [26] is a representative method to select the ISFB of the SCoh for constructing diagnostic IES. It splits the entire spectral frequency band of the SCoh into a 1/3-binary tree form, like

the fast Kurtogram method [5], to create a group of candidate sub-bands with different central frequencies and bandwidths, as displayed in Fig. 1. A total of 2^k narrow bands with equal bandwidths can be obtained at the kth ($k = 0,1,1.6,2,2.6,3,\cdots$) level. For the ith ($i = 1,2,3,\cdots,2^k$) narrow band at the kth level, the center frequency and its bandwidth are, respectively, expressed as follows:

$$f_{k,i} = F_s \cdot \left(i - 2^{-1}\right) \big/ 2^{k+1} \tag{6}$$

$$\Delta f_k = F_s \big/ 2^{k+1} \tag{7}$$

The starting frequency f_1 and ending frequency f_2 of this narrow band can be defined as:

$$\begin{cases} f_1 = f_{k,i} - \Delta f_k / 2 = F_s \cdot (i-1) \big/ 2^{k+1} \\ f_2 = f_{k,i} + \Delta f_k / 2 = F_s \cdot i \big/ 2^{k+1} \end{cases} \tag{8}$$

Then, the IES generated from this spectral frequency band can be formulated as:

$$\mathrm{IES}_{k,i}(\alpha) = \frac{1}{F_s / 2^{k+1}} \int_{F_s \cdot (i-1)/2^{k+1}}^{F_s \cdot i / 2^{k+1}} \left| \gamma_x(\alpha, f) \right| df \tag{9}$$

A feature indicator is devised to assess the failure-relevant information contained in these candidate IESs and the spectral frequency band with the largest feature indicator is identified as an optimal ISFB to generate diagnostic IES. For visual observation, the feature indicators of different frequency bands can be drawn into a two-dimensional color map, called IESFOgram. Please refer to [26] for the detailed introduction of the IESFOgram.

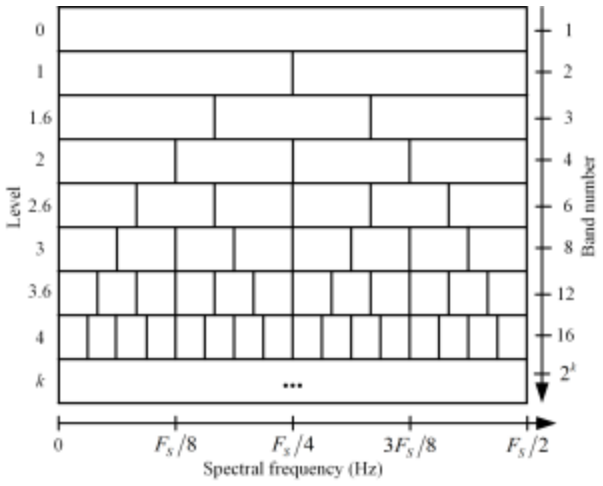

Fig. 1. Spectral frequency band division in the form of 1/3-binary tree.

3. Blind and targeted features for frequency band selection

This section first briefly discusses the typical blind features and targeted features that disclose the cyclostationarity of bearing failure symptoms. Their performance in identifying the ISFB of SCoh is investigated in this paper. Then, a novel targeted feature dedicated to evaluating the SNR in the cyclic frequency domain is proposed to distinguish an ISFB of SCoh for fault diagnosis.

3.1. Blind features for frequency band selection

Sparsity measures are typical blind features that characterize bearing fault information in the frequency domain or time domain and are widely employed as frequency band selection criteria in

envelope analysis, mainly including Kurt [5,6], NE [7], L2/L1 norm [8], HI [14], RSI [10,13] and GI [11]. Among these blind features, only the L2/L1 norm has been used to identify the ISFBs of SCoh to construct fault-sensitive IESs [24], while the performance of other blind features in SCoh-based bearing fault diagnosis has not been studied and verified. Therefore, they are introduced into the identification of the ISFB of SCoh in this paper, and their performance in bearing fault diagnosis is systematically verified and compared.

Assuming that $\mathrm{IES}_{k,i}[n]$ is the discrete form of IES generated in the ith narrow band of the kth level, where $n=1,2,\cdots,L$ and L is the total number of discrete cyclic frequencies, the typical blind features (i.e., sparsity measures) for frequency band selection are formulated as follows.

Blind feature 1: Kurtosis

$$\mathrm{Kurt}_{k,i}=\frac{\left\langle \mathrm{IES}_{k,i}[n]^4 \right\rangle}{\left\langle \mathrm{IES}_{k,i}[n]^2 \right\rangle^2} \tag{10}$$

where symbol $\langle\cdot\rangle$ denotes the mean operator.

Blind feature 2: Negentropy

$$\mathrm{NE}_{k,i}=\left\langle \frac{\mathrm{IES}_{k,i}[n]^2}{\left\langle \mathrm{IES}_{k,i}[n]^2 \right\rangle} \ln\left(\frac{\mathrm{IES}_{k,i}[n]^2}{\left\langle \mathrm{IES}_{k,i}[n]^2 \right\rangle} \right) \right\rangle \tag{11}$$

Blind feature 3: Ratio of L2 norm to L1 norm

$$\mathrm{L2/L1}_{k,i}=\frac{\left\| \mathrm{IES}_{k,i}[n] \right\|_2}{\left\| \mathrm{IES}_{k,i}[n] \right\|_1} \tag{12}$$

where symbols $\|\cdot\|_1$ and $\|\cdot\|_2$ are the L1 and L2 norms, respectively.

Blind feature 4: Hoyer index

$$\mathrm{HI}_{k,i}=\frac{1}{\sqrt{L}-1}\left(\sqrt{L}-\frac{\left\| \mathrm{IES}_{k,i}[n] \right\|_1}{\left\| \mathrm{IES}_{k,i}[n] \right\|_2} \right) \tag{13}$$

Blind feature 5: Reciprocal of smoothness index

$$\mathrm{RSI}_{k,i}=\frac{\left\langle \mathrm{IES}_{k,i}[n] \right\rangle}{\sqrt[L]{\prod_{n=1}^{L}\mathrm{IES}_{k,i}[n]}} \tag{14}$$

Blind feature 6: Gini index

$$\mathrm{GI}_{k,i}=1-\sum_{n=1}^{L}\frac{\mathrm{IES}_{k,i}^{r}[n]}{\left\| \mathrm{IES}_{k,i}[n] \right\|_1}\frac{2(L-n)+1}{L} \tag{15}$$

where $\mathrm{IES}_{k,i}^{r}[n]$ is the ascending sequence of the amplitudes of $\mathrm{IES}_{k,i}[n]$, i.e., $\mathrm{IES}_{k,i}^{r}[1]\le \mathrm{IES}_{k,i}^{r}[2]\le\cdots\le \mathrm{IES}_{k,i}^{r}[L]$.

3.2. Targeted features for frequency band selection

The targeted features are usually constructed from the amplitude of the specified characteristic frequency and its several harmonics and are applied to quantify the cyclostationary components relevant to the specified defect in the frequency domain. Some targeted features have recently been developed to select the ISFB of SCoh to generate diagnostic IES, mainly including the Ind [26],

diagnostic feature (DF) [27], spectral density (SD) [26] and SNR measure [33]. However, different band division strategies are used to decompose the spectral frequency band of SCoh. In addition, the RCC [17] and ICS2 [16] are two representative indicators for measuring the targeted cyclostationary components in the frequency domain. In this study, they are introduced into the identification of the ISFB of SCoh, and their performance in bearing fault diagnosis is verified and compared with other targeted features.

The typical targeted features for frequency band selection are defined as follows.

Targeted feature 1: Ind (the summation of the amplitude of a specified characteristic frequency and its several harmonics) [26]

$$\mathrm{Ind}_{k,i} = \sum_{h=1}^{H} \max_{n \in A_h} \left(\mathrm{IES}_{k,i}[n] \right) \tag{16}$$

where H represents the number of the considered harmonics, A_h denotes a series of cyclic frequencies in a small band around the hth harmonic of the detected characteristic frequency.

Targeted feature 2: Diagnostic feature [27]

$$\mathrm{DF}_{k,i} = \sum_{h=1}^{H} \frac{\max_{n \in A_h} \left(\mathrm{IES}_{k,i}[n] \right)}{\left[\sum_{n \in B_h} \mathrm{IES}_{k,i}[n] - \max_{n \in A_h} \left(\mathrm{IES}_{k,i}[n] \right) \right] \Big/ \left[num(B_h) - 1 \right]} \tag{17}$$

where B_h denotes a series of cyclic frequencies in a small band around the hth harmonic of the detected frequency component and is slightly wider than the tolerance band A_h; $num(B_h)$ represents the number of cyclic frequencies in the tolerance band B_h.

Targeted feature 3: Spectral density (the product of the amplitude of a specified characteristic frequency and its several harmonics) [26]

$$\mathrm{SD}_{k,i} = \prod_{h=1}^{H} \max_{n \in A_h} \left(\mathrm{IES}_{k,i}[n] \right) \tag{18}$$

Targeted feature 4: Signal-to-noise ratio measure [33]

$$\mathrm{SNR}_{k,i} = \sum_{h=1}^{H} \frac{\max_{n \in A_h} \left(\left| \mathrm{IES}_{k,i}[n] \right|^2 \right)}{median_{n \in B_h} \left(\left| \mathrm{IES}_{k,i}[n] \right|^2 \right)} \tag{19}$$

where $median(\cdot)$ denote the median operator and is employed to estimate the noise intensity.

Targeted feature 5: Ratio of cyclic content [17]

$$\mathrm{RCC}_{k,i} = \frac{\sum_{h=1}^{H} \sum_{n \in A_h} \left| \mathrm{IES}_{k,i}[n] \right|^2}{\sum_{n=1}^{L} \left| \mathrm{IES}_{k,i}[n] \right|^2} \tag{20}$$

Targeted feature 6: Indicator of second-order cyclostationarity [16]

$$\mathrm{ICS2}_{k,i} = \frac{\sum_{h=1}^{H} \max_{n \in A_h} \left(\left| \mathrm{IES}_{k,i}[n] \right|^2 \right)}{\left| \mathrm{IES}_{k,i}[0] \right|^2} \tag{21}$$

3.3. Proposed targeted feature for frequency band selection

In this section, a novel targeted feature named frequency domain signal-to-noise ratio (FDSNR) is devised to evaluate the failure information in the cyclic frequency domain. FDSNR is defined as the ratio of the average energy of the fault-related components to the average energy of the noise components, as shown in Eq. (22).

Targeted feature 7: Frequency domain signal-to-noise ratio

$$\mathrm{FDSNR}_{k,i}=\frac{\frac{1}{H}\sum_{h=1}^{H}\max_{n\in A_h}\left(\left|\mathrm{IES}_{k,i}[n]\right|^2\right)}{\frac{1}{L-H}\left(\sum_{n=1}^{L}\left|\mathrm{IES}_{k,i}[n]\right|^2-\sum_{h=1}^{H}\max_{n\in A_h}\left(\left|\mathrm{IES}_{k,i}[n]\right|^2\right)\right)} \tag{22}$$

Compared with Ind and SD, FDSNR considers normalization to overcome the influence of interference components, and compared with RCC and ICS2, FDSNR is more robust to interference components. Taking FDSNR as the fault information measure, an enhanced method is developed in this article to distinguish an optimal spectral frequency band of SCoh for constructing diagnostic IES. A schematic diagram of the proposed methodology for bearing diagnostics is shown in Fig. 2. The main procedure of the proposed methodology is described as follows:

Step 1: Acquire bearing vibration acceleration signals from the monitored rotating machinery.

Step 2: Estimate the SCoh of bearing vibration acceleration data following the fast SC numerical algorithm [23] by setting the appropriate window length and maximum observed cyclic frequency.

Step 3: Divide the full spectral frequency band of the SCoh into a group of narrow bands using a 1/3-binary tree division technology. Then, construct a series of candidate IESs by integrating the SCoh over different spectral frequency bands and calculate their FDSNR values to evaluate the fault information contained in the narrow bands.

Step 4: Identify the IES with the largest FDSNR value as the optimal demodulated spectrum and employ it to perform bearing defect diagnostics.

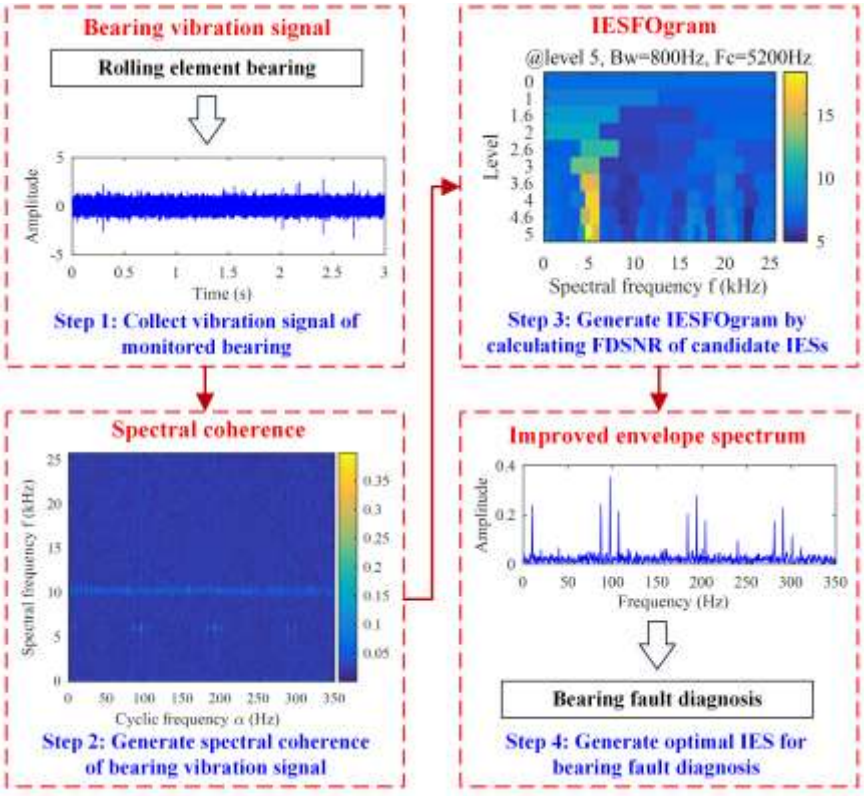

Fig. 2. Schematic diagram of the developed methodology for bearing defect diagnostics.

4. Comparison on simulated bearing failure data

In this section, the frequency band selection and fault detection performance of typical blind

features, typical targeted features and FDSNR, as the fault information measure of IESFOgram, is validated and compared on simulated bearing failure datasets with diverse interference noises.

4.1. Simulation model of bearing failure data

The simulated signals are generated from a bearing fault numerical model. According to the signal model in [19], the numerical model is formulated as:

$$x_{BF}(t)=\sum\nolimits_m A_m \cdot O(t-mT-\tau_m)+x_{GWN}(t)+B\cdot x_{INT}(t) \tag{23}$$

The first item simulates the typical impulse signal induced by a spalling on bearing inner race, where T is the nominal value of impulse period, τ_m denotes the tiny fluctuation of the occurrence time of the mth fault impulse due to roller sliding and is generated from a uniform distribution $U(T,2T)/100$, A_m indicates the amplitude of mth fault impulse and is specified as $A_m=(1-\cos(2\pi f_r t))/2$, and f_r represents the rotation frequency of the shaft. $O(t)$ simulates transient impulse characterized by the damping ratio ς and resonant frequency f_n, and can be formulated as [19]:

$$O(t)=e^{-2\pi\varsigma f_n t}\sin\left(2\pi\sqrt{1-\varsigma^2}\,f_n t+\varphi_0\right) \tag{24}$$

where φ_0 represents the initial phase. Table 1 presents the specific parameters of the fault simulation component of bearing inner race.

The second item $x_{GWN}(t)$ indicates the background noise component from the operating environment. In this article, the Gaussian white noise is used as the background noise and is added to the bearing fault signal to generate an SNR of –10 dB. The third item $B\cdot x_{INT}(t)$ denotes the typical non-Gaussian interference noise, such as the impulsive cyclostationary noise caused by the damage of other rotating components and random impulsive noise caused by external shocks, scaled by coefficient B to simulate different noise levels. Suppose the sampling duration and sampling rate are 3 s and 51.2 kHz, respectively. In this study, simulation analysis and experimental analysis are conducted in the MATLAB R2016b environment. The typical interference noises utilized in simulation analysis are introduced as follows:

- ***Gaussian white noise***: generated from the AWGN function in MATLAB platform.
- ***Impulsive cyclostationary noise***: generated from the same model as the impulsive fault component in Eq. (23), but is assigned a characteristic frequency of 40 Hz and a constant amplitude of 0.5. The resonance frequency, damping ratio, and initial phase are specified as 10 kHz, 0.02, and 0°, respectively.
- ***Random impulsive noise***: generated from the same model as the impulsive fault component in Eq. (23), but its amplitude and occurrence time are obtained from a Gaussian distribution $N(1.5,1)$ and a uniform distribution $U(0,3)$, respectively. The resonance frequency, damping ratio, and initial phase are set to 10 kHz, 0.02, and 0°, respectively.

Fig. 3 displays the waveforms of the different components of bearing vibration signal. Note that only the signal waveform of 0.5 s is depicted to facilitate the observation.

Table 1. Specific parameters of the fault simulation component of bearing inner race.

Parameter	f_r (Hz)	f_n (Hz)	ς	φ_0 (°)	T (s)
Value	10	5800	0.02	0	1/97

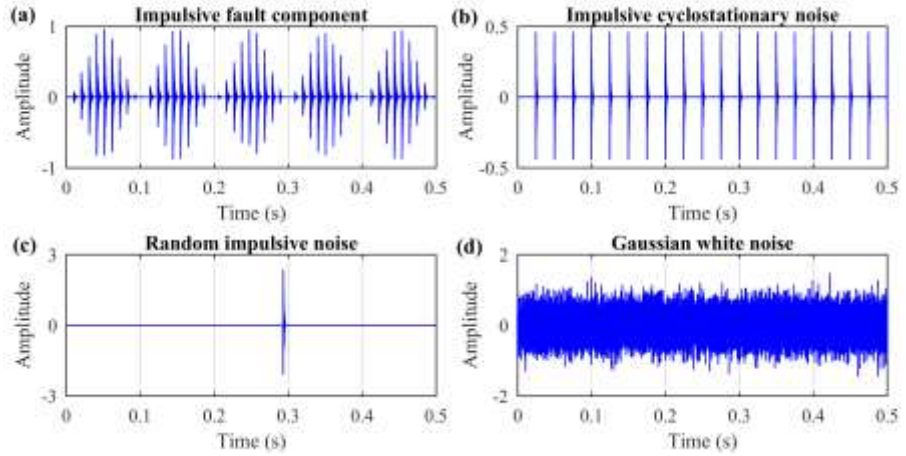

Fig. 3. Components of bearing vibration signals: (a) impulsive fault component, (b) impulsive cyclostationary noise, (c) random impulsive noise, and (d) Gaussian white noise.

4.2. Results on simulated bearing fault signals

The band selection and fault detection performance of the IESFOgram using typical blind features (Kurt, NE, L2/L1, HI, RSI and GI), typical targeted features (Ind, DF, SD, SNR, RCC, and ICS2) and FDSNR is validated and compared on the simulated bearing fault signals generated in Sections 4.1. The spectral frequency bands selected by each method under different noise levels are plotted as a two-dimensional map for comparison. In addition, the FDSNR value of the resulting IES is employed to quantitatively assess the fault detection effects of the IESFOgram using diverse features under different noise levels.

To estimate the SCoh and generate the IESFOgram, the input parameters should be selected reasonably. The key parameters of the fast SC estimator [23] include the window length N_w and the maximum observed cyclic frequency $\alpha_{\max}$. To accurately identify bearing faults, the maximum observed cyclic frequency $\alpha_{\max}$ should be greater than 3 times the detected characteristic frequency. In this section, $\alpha_{\max}$ is specified as 350 Hz to cover three harmonics of the detected characteristic frequency. The window length N_w governs the spectral frequency resolution. To facilitate the division of the entire spectral frequency band into a 1/3-binary tree form, the window length is designated as $N_w = 3 \cdot 2^{K+1}$ in this study, where K is the decomposition level as shown in Fig. 1. The window length N_w should be much smaller than the signal length while ensuring the proper spectral frequency resolution [23,34]. The decomposition level K is set as 5 in this section, therefore the window length N_w is specified as 192 sampling points. Additionally, to estimate the targeted features, the detected characteristic fault frequency and its first two harmonic components are considered in this study, i.e., $H = 3$, and the tolerance bands A_h and B_h respectively contain 3 and 5 spectral lines on both sides of the harmonic of nominal fault characteristic frequency.

4.2.1. Results on bearing fault signals with different Gaussian white noise levels

In this case, the generated bearing defect signals are only polluted by the Gaussian white noise, and other interference sources are ignored. The intensity of the added Gaussian white noise is regulated with SNR from −30 to 0 dB in 1 dB increments.

The IESFOgram using typical blind features, typical targeted features and FDSNR are employed to each bearing fault simulation signature, and the spectral frequency bands selected under diverse Gaussian white noise levels are respectively presented in Figs. 4, 5 and 6(a). Fig. 4 displays the band

selection results of the blind feature-based methods. When the noise intensity is greater than –10 dB or –9 dB, all blind feature-based methods basically select the entire spectral frequency band of the SCoh; as the SNR decreases, they select a narrow spectral frequency band around the bearing resonant frequency; however, when the noise intensity is lower than the cut-off noise level (about –18 dB for the Kurt, NE, L2/L1 and HI, –16 dB for the RSI, and –17 dB for the GI), they cannot accurately distinguish the resonant frequency band of the simulated bearing failure component. For the targeted feature-based methods and the presented approach, when the noise intensity is greater than the cut-off noise level (about –19 dB for the Ind, DF, SD, SNR, ICS2 and FDSNR, and –21 dB for the RCC), all targeted feature-based methods and the proposed method select a narrow spectral frequency band around the bearing resonant frequency; when the noise intensity is lower than the cut-off noise level, the spectral frequency bands selected are far from the resonant frequency of the simulated bearing failure component. Fig. 6(b) displays the resulting IESs of the presented approach for processing the simulation signals with diverse Gaussian white noise levels. The fault characteristic frequencies 97 Hz, 194 Hz and 291 Hz can be clearly detected from the generated IES when the noise intensity is higher than –19 dB. Fig. 7 shows the FDSNR obtained by IESFOgram with different features under different Gaussian white noise levels. The FDSNR achieved by the proposed approach is basically the same as the FDSNR of the targeted feature-based methods and is greater than the FDSNR of the blind feature-based methods. These results indicate that the band selection and fault detection effect of the developed approach is similar to that of the targeted feature-based methods and is better than that of the blind feature-based methods under the interference of Gaussian white noise.

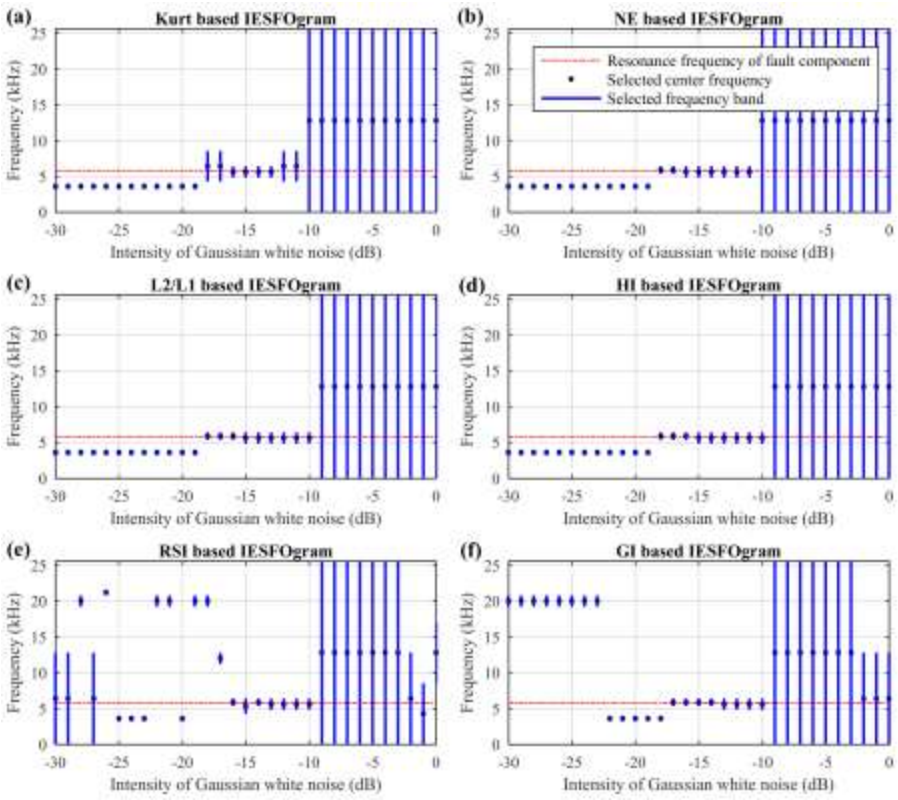

Fig. 4. Spectral frequency bands selected by IESFOgram with blind features under different Gaussian white noise levels.

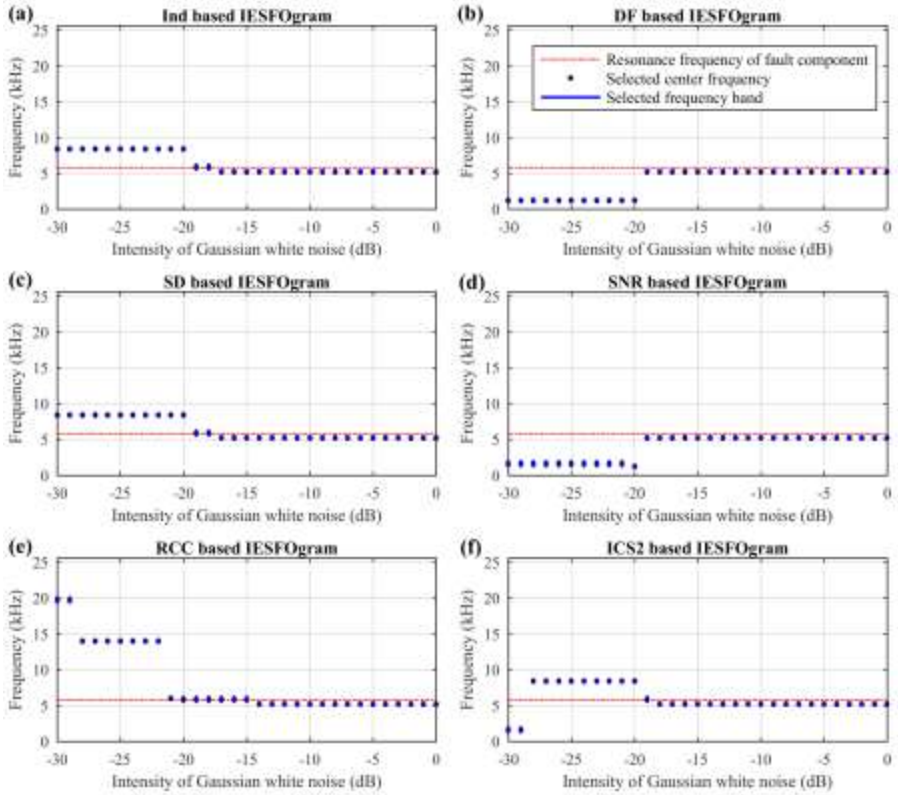

Fig. 5. Spectral frequency bands selected by IESFOgram with targeted features under different Gaussian white noise levels.

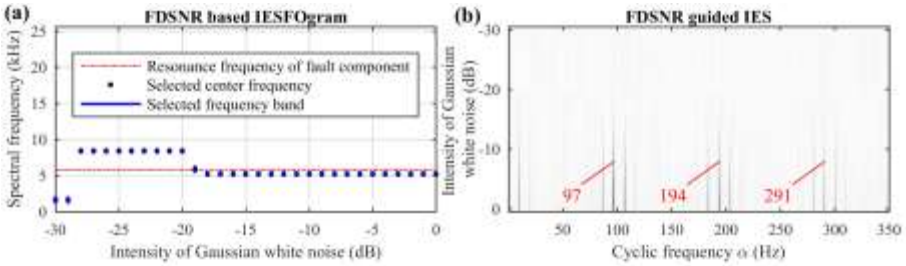

Fig. 6. Results of IESFOgram using FDSNR under different Gaussian white noise levels: (a) selected spectral frequency bands, and (b) generated improved envelope spectra (white = 0, black = 1).

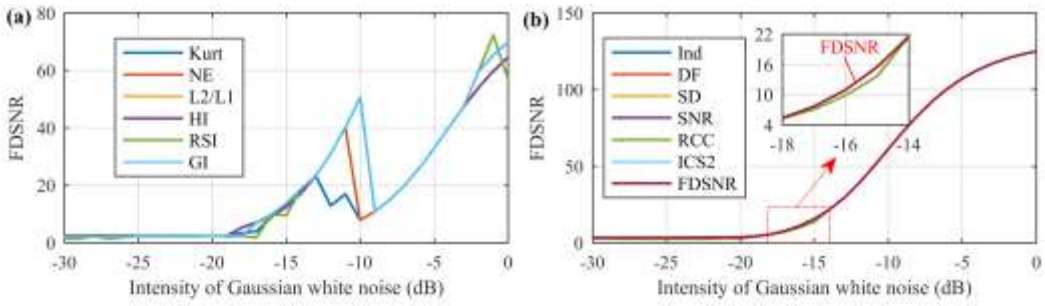

Fig. 7. FDSNR obtained by IESFOgram with different features under different Gaussian white noise levels: (a) blind features and (b) targeted features.

4.2.2. Results on bearing fault signals with different impulsive cyclostationary noise levels

In this case, the white Gaussian noise with an SNR of –10 dB and the impulsive cyclostationary noise are added to contaminate the bearing fault component. The coefficient B in Eq. (23) was adjusted from 0.2 to 8 in 0.2 increments.

Figs. 8, 9 and 10(a) display the frequency band selection results of the IESFOgram using typical blind features, typical targeted features and FDSNR, respectively. The blind feature-based methods can discriminate the resonant frequency band of the bearing defect component only when the amplitude of the impulsive cyclostationary noise is less than the cut-off amplitude level (about 1.4 for the Kurt, and 1 for the NE, L2/L1, HI, RSI and GI). Note that although the entire spectral frequency band is selected by the Kurt-based method when the noise amplitude is less than 1 and is selected by the RSI and GI-based methods when the noise amplitude is higher than 4.2, the generated IESs are dominated by the characteristic frequency and its first several harmonic components of the bearing defect simulation component and impulsive cyclostationary noise, respectively. In contrast, the targeted feature-based methods and the proposed method exhibit better resistance to impulsive cyclostationary noise. As the amplitude of the impulsive cyclostationary noise increases from 0.2 to 8, the selected spectral frequency band stabilizes around the resonance frequency of the bearing defect simulation signal, and the interested characteristic frequencies 97 Hz, 194 Hz and 291 Hz can be clearly distinguished from the resulting IESs, as exhibited in Fig. 10(b). In Fig. 11, the FDSNR of the proposed method is consistent with that of the targeted feature-based methods and is greater than the FDSNRs of the blind feature-based approaches. These results disclose that the presented approach and the targeted feature-based approaches have similar ability to resist the impulsive cyclostationary noise and are more robust than the blind feature-based methods.

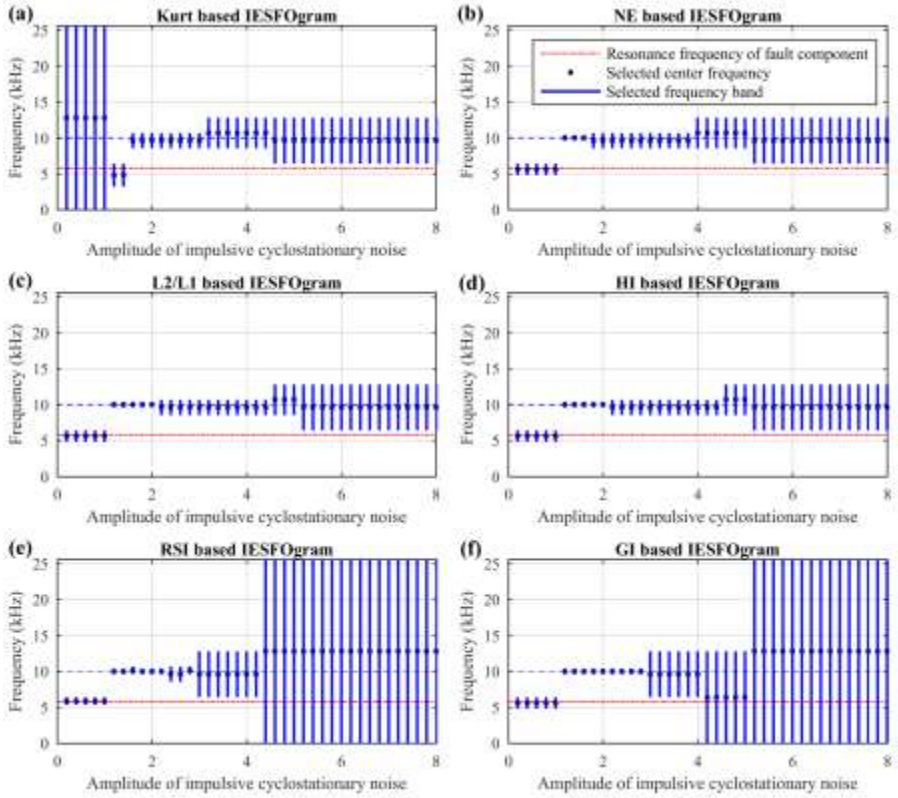

Fig. 8. Spectral frequency bands selected by IESFOgram with blind features under different impulsive cyclostationary noise levels. (blue dashed line indicates the resonance frequency of impulsive cyclostationary

noise).

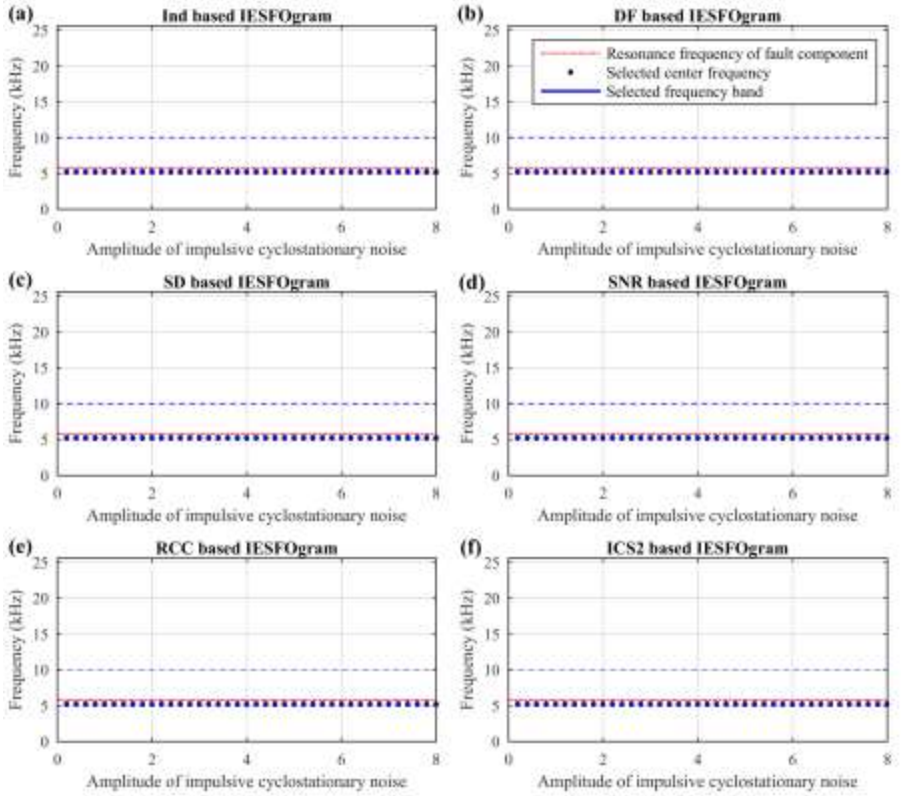

Fig. 9. Spectral frequency bands selected by IESFOgram with targeted features under different impulsive cyclostationary noise levels. (blue dashed line indicates the resonance frequency of impulsive cyclostationary noise).

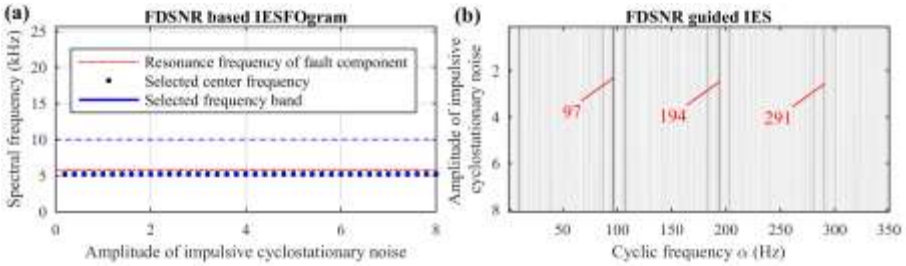

Fig. 10. Results of IESFOgram using FDSNR under different impulsive cyclostationary noise levels: (a) selected spectral frequency bands (blue dashed line indicates the resonance frequency of impulsive cyclostationary noise), and (b) generated improved envelope spectra (white = 0, black = 1).

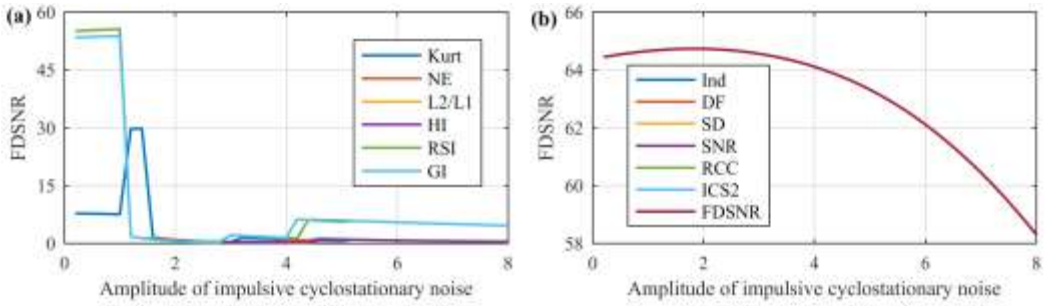

Fig. 11. FDSNR obtained by IESFOgram with different features under different impulsive cyclostationary noise levels: (a) blind features and (b) targeted features.

4.2.3. Results on bearing fault signals with different random impulsive noise levels

In this case, the white Gaussian noise with an SNR of –10 dB and the random impulsive noise are added to contaminate the bearing fault component. The coefficient B in Eq. (23) was adjusted from 0.25 to 12 in 0.25 increments.

Figs. 12, 13 and 14(a) display the frequency band selection results of the IESFOgram using typical blind features, typical targeted features and FDSNR, respectively. For the blind feature-based methods, as the amplitude of random impulsive noise increases from 0.25 to the cut-off amplitude level (about 10 for the Kurt, 9.25 for the NE, 8.75 for the L2/L1 and HI, 6.75 for the RSI, and 8.25 for the GI), the spectral frequency bands selected are mainly concentrated around the bearing resonance frequency; however, when the amplitude is larger than the cut-off amplitude level, the spectral frequency bands selected are unstable. For the targeted feature-based methods, the DF, SNR, RCC and FDSNR-based methods deliver stronger resistance to random impulse noise in comparison with the Ind, SD and ICS2-based methods, judging from the cut-off amplitude levels of these targeted features (about 2 for the Ind, SD and ICS2, 9.75 for the DF and SNR, 10.75 for the RCC, and 11 for the FDSNR). As described in Fig. 14(b), the interested characteristic frequencies 97 Hz, 194 Hz and 291 Hz can be clearly identified from the resulting IES when the amplitude of the random impulsive noise is lower than 11. Fig. 15 displays the FDSNR of IESFOgram using blind and targeted features under different random impulsive noise levels. It can be discovered that the FDSNR of the developed approach is similar to the FDSNRs of the DF, SNR and RCC-based methods and is larger than that of the blind feature-based methods and the Ind, SD and ICS2-based methods. These results demonstrate that the band selection and fault detection capability of the presented approach and the DF, SNR and RCC-based methods are superior to that of the blind feature-based methods and the Ind, SD and ICS2-based methods in the presence of strong random impulses.

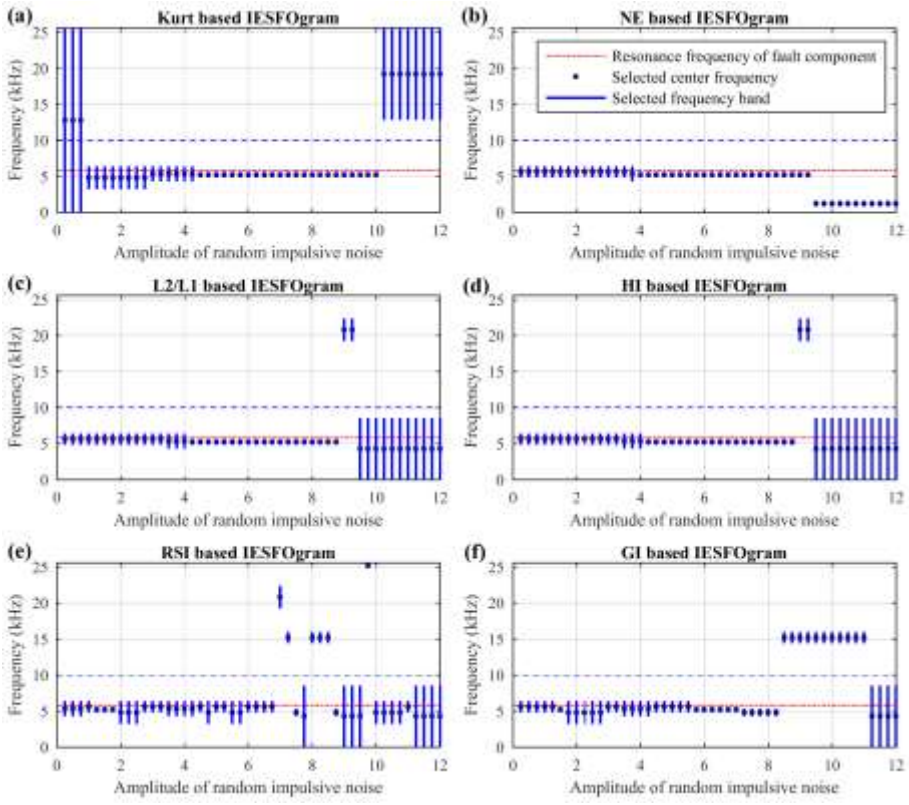

Fig. 12. Spectral frequency bands selected by IESFOgram with blind features under different random impulsive

noise levels. (blue dashed line indicates the resonance frequency of random impulsive noise).

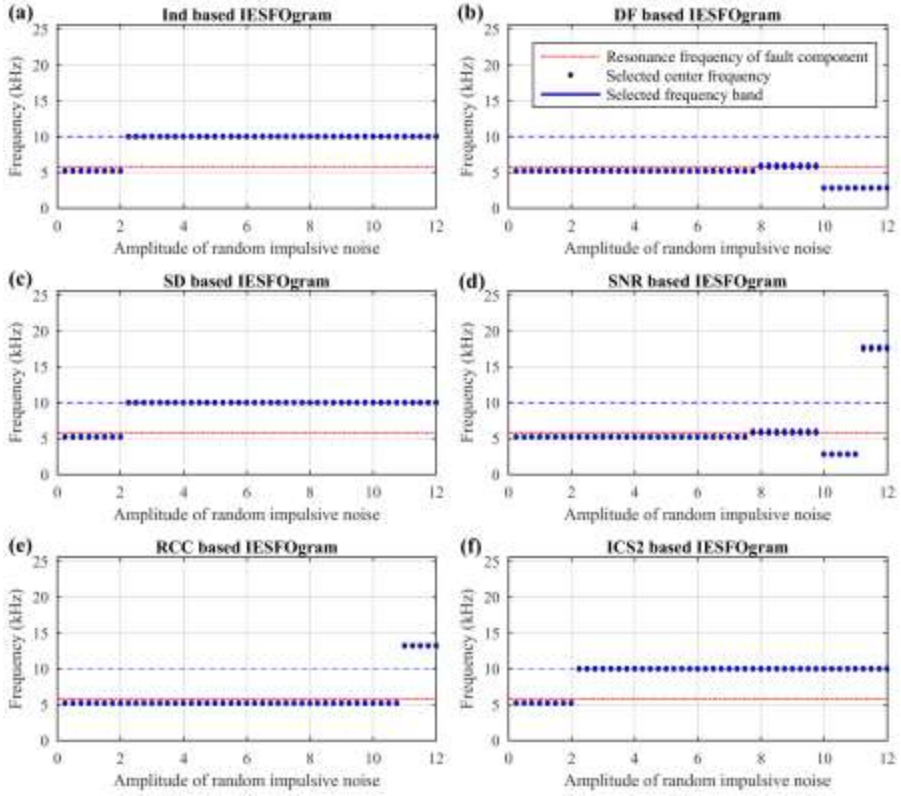

Fig. 13. Spectral frequency bands selected by IESFOgram with targeted features under different random impulsive noise levels. (blue dashed line indicates the resonance frequency of random impulsive noise).

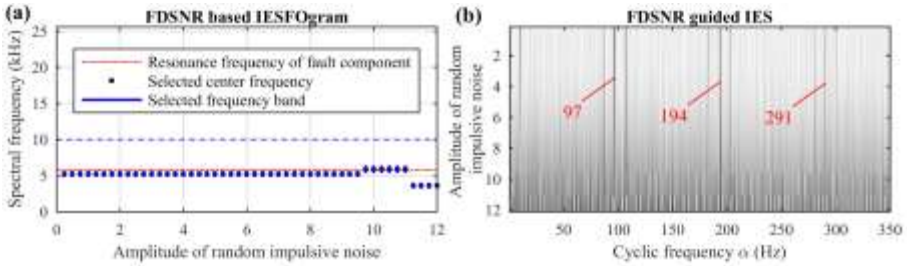

Fig. 14. Results of IESFOgram using FDSNR under different random impulsive noise levels: (a) selected spectral frequency bands (blue dashed line indicates the resonance frequency of random impulsive noise), and (b) generated improved envelope spectra (white = 0, black = 1).

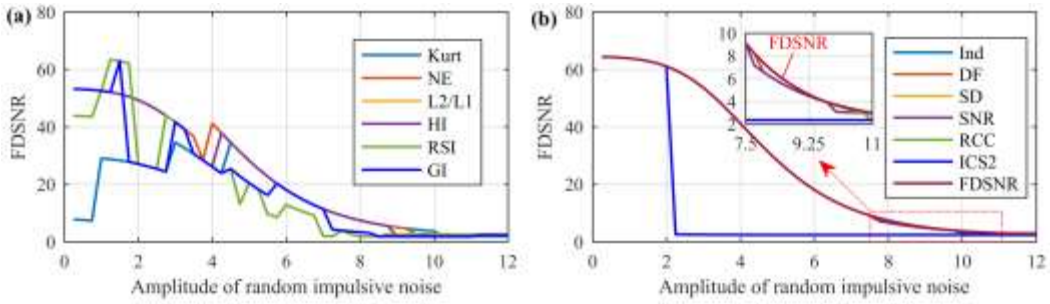

Fig. 15. FDSNR obtained by IESFOgram with different features under different random impulsive noise levels: (a) blind features and (b) targeted features.

4.3. Summary of comparison results on simulated signals

The frequency band selection and performance analysis results of the blind feature-based methods, the targeted feature-based methods and the proposed method on simulated bearing fault signals show that:

- The blind features focus on global information and the methods based on them tend to select a relatively wide ISFB of the SCoh, while the targeted features focus on local information and the methods based on them tend to select a relatively narrow ISFB.
- The NE, L2/L1 and HI-based methods exhibit similar band selection and defect identification performance under the interference of Gaussian white noise, random impulse noise and impulsive cyclostationary noise, and are slightly better than the RSI and GI-based methods. Compared with other blind feature-based methods, the Kurt-based method is susceptible to impulsive cyclostationary noise and random impulsive noise.
- The proposed method and the targeted feature-based methods deliver similar band selection and fault detection performance under the interference of impulsive cyclostationary noise and Gaussian white noise and outperform the blind feature-based approaches. Under the interference of random impulse noise, the effect of the Ind, SD and ICS2-based methods is inferior to that of the proposed method and the DF, SNR and RCC-based methods due to no or inappropriate normalization.
- The fault detection performance of the proposed method and the DF, SNR and RCC-based methods is superior to that of the blind feature-based methods and the Ind, SD and ICS2-based methods under the presence of Gaussian noise and typical non-Gaussian noises.

5. Comparison on bearing experimental signals

In this section, the band selection and fault detection performance of the IESFOgram using typical blind features, typical targeted features and FDSNR is validated and compared on three bearing experimental signals. The results (gram and IES) of the IESFOgram using state-of-the-art features and FDSNR for the bearing experimental signals are presented for comparison. The maximum observed cyclic frequency of the SCoh is set to cover the detected bearing characteristic frequency and its first two harmonic components. The decomposition level of the spectral frequency band is set to 6, and the window length utilized to estimate the SCoh of bearing vibration signal is 384 samples.

5.1. Planetary bearing outer race defect detection

The first bearing experimental data [37] was acquired from a planetary gearbox test rig of the University of New South Wales (UNSW), Australia. The tested gearbox mainly contains a parallel gear system, in which a spur gear integrated with the planet carrier is driven by a pinion gear, as depicted in Fig. 16(a). A localized defect was implanted into the outer race of a planetary bearing (IKO model NAF 122812), as displayed in Fig. 16(b). An acceleration sensor mounted above the stationary ring gear was used for the acquisition of vibration signals at a sampling rate of 150 kHz. During data acquisition, the input shaft of planetary gearbox rotated at a constant speed of about 324 r/min. The ball pass frequency of outer race (BFPO) of the planetary bearing is about 66.42 Hz, with a modulation frequency of 14.36 Hz. A detailed introduction of the experiment can be found in [20].

Fig. 17 (a) and (b) depict respectively the measured vibration acceleration data and its magnitude spectrum. From the SES of the vibration signal presented in Fig. 17(c), the spectral peaks at BPFO of the planetary bearing and its harmonics (marked with red dot line) cannot be detected. Set the

maximum cyclic frequency of observation to 300 Hz. The SCoh and EES are respectively exhibited in Fig. 17(d) and (e). Because of the complex interference noises, the BPFO of the planetary bearing and its harmonics still cannot be identified.

The IESFOgram method using blind features and targeted features is employed to deal with the vibration signature exhibited in Fig. 17(a), and the corresponding results (gram and IES) are displayed in Figs. 18 and 19, respectively. The resulting IESs depicted in Fig. 18 exhibit high impulsiveness due to the dominated spectral peaks at the modulation frequency component and its harmonic components, while the spectral lines at the characteristic frequencies induced by the bearing defect cannot be observed. These results suggest that the blind feature-based methods fail to distinguish the resonance frequency band induced by the planetary bearing defect. For the targeted feature-based methods, the spectral peaks at the BPFO and its first two harmonic components can be distinguished in the IESs displayed in Fig. 19(b), (d) and (e), indicating that only the DF, SNR and RCC-based methods successfully recognize the defect-triggered resonance frequency band. The failure of the Ind, SD, and ICS2-based methods to correctly determine the ISFB may be caused by the non-normalization or inappropriate normalization of these targeted features.

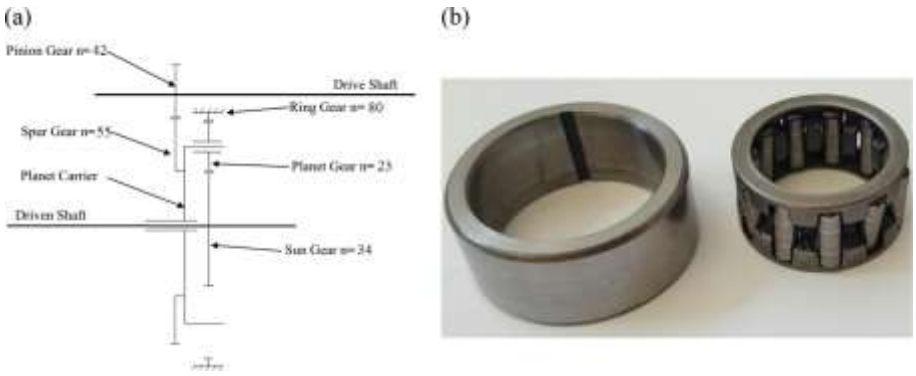

Fig. 16. (a) Diagram of the UNSW planetary gearbox test rig and (b) planetary bearing with seeded fault [20].

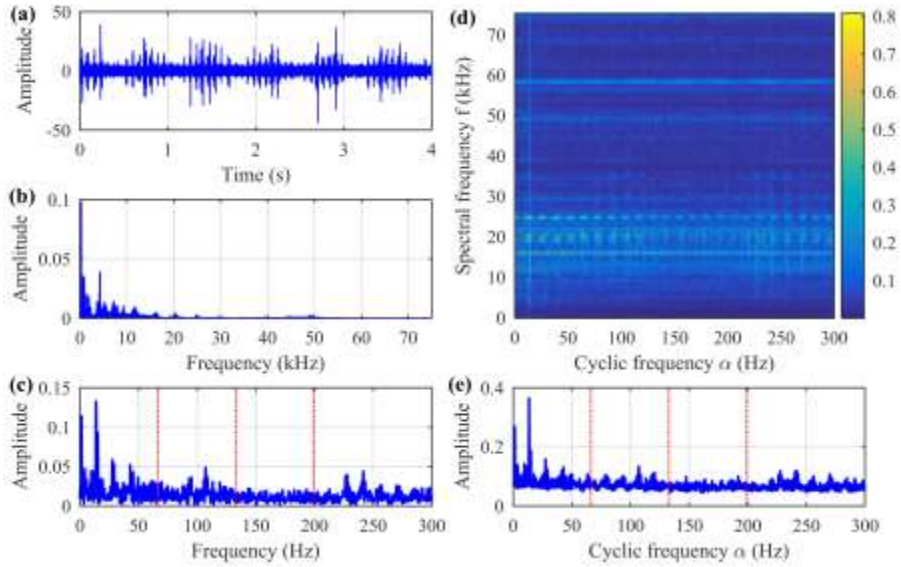

Fig. 17. Results of planetary gearbox bearing defect signature: (a) signal waveform, (b) magnitude spectrum, (c) SES, (d) SCoh, and (e) EES.

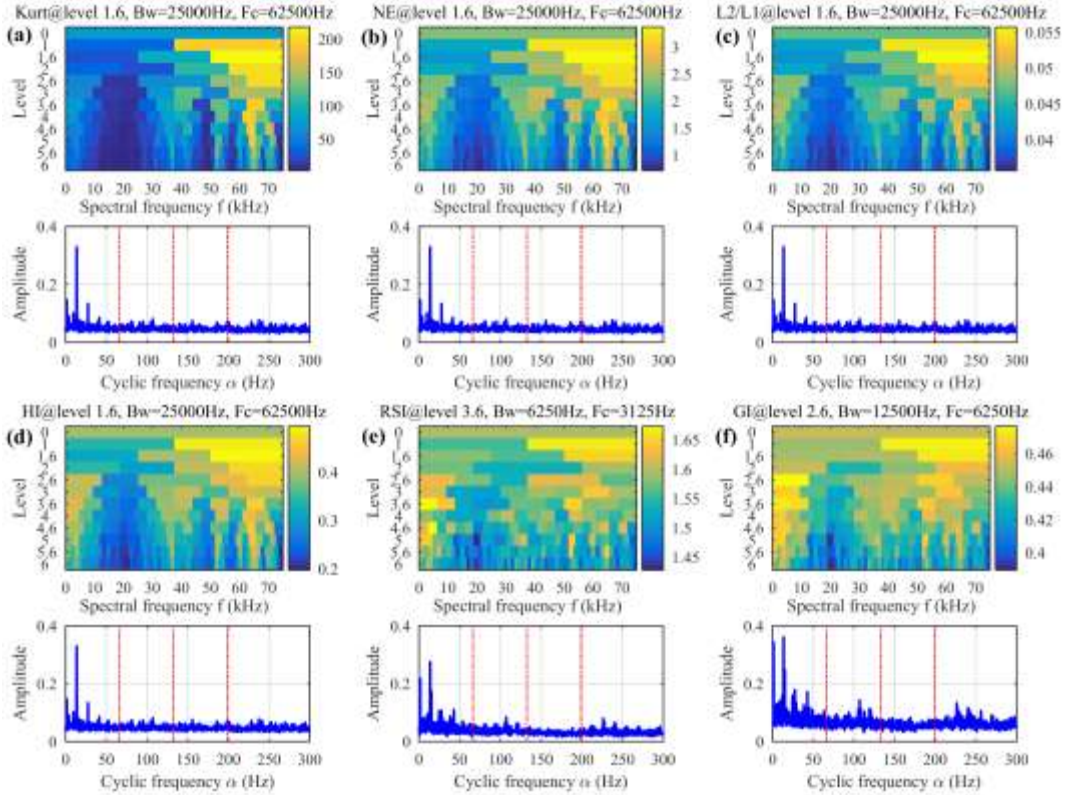

Fig. 18. Results (gram and IES) of IESFOgram based on blind features for the planetary gearbox bearing defect signature: (a) Kurt, (b) NE, (c) L2/L1, (d) HI, (e) RSI, and (f) GI.

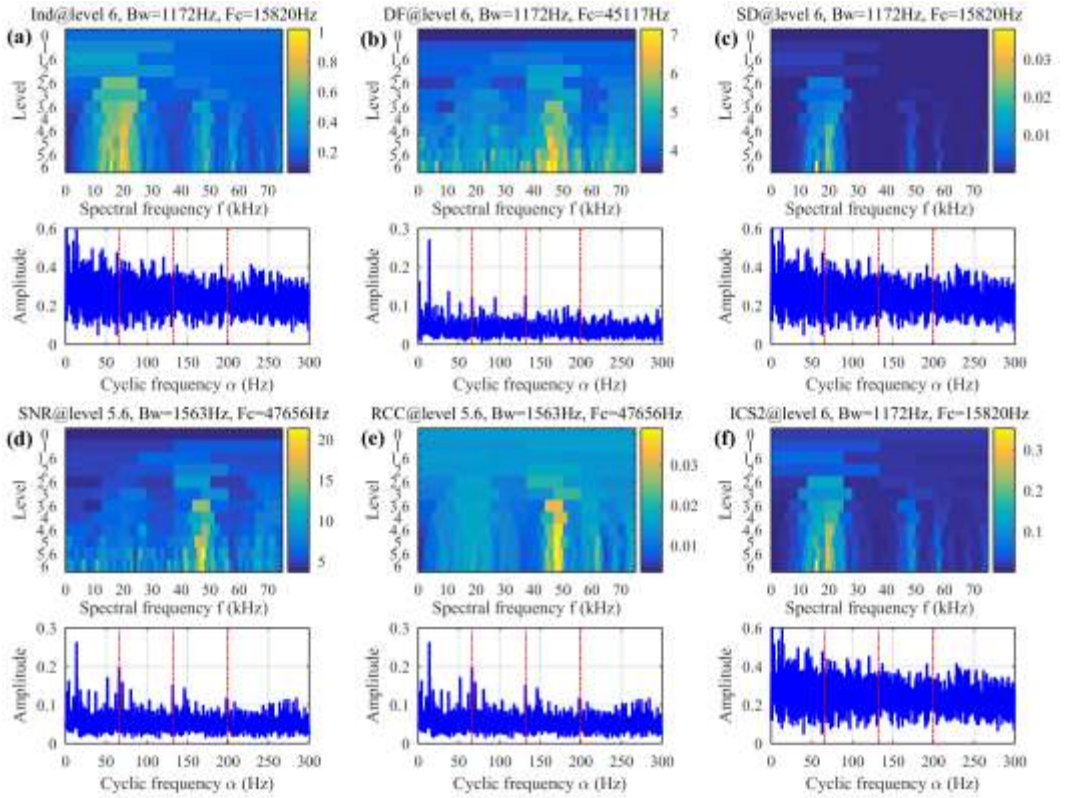

Fig. 19. Results (gram and IES) of IESFOgram based on targeted features for the planetary gearbox bearing defect signature: (a) Ind, (b) DF, (c) SD, (d) SNR, (e) RCC, and (f) ICS2.

5.2. Rolling bearing outer race defect detection

The second experimental data [38] was collected from the bearing test rig of the University of Electronic Science and Technology of China (UESTC). The test rig is mainly composed of the motor and speed controller, support bearing, loading disc and test bearing, as displayed in Fig. 20. A local defect was implanted into the outer race of the test bearing. In this experiment, the spindle rotated at a constant speed of 600 r/min (10 Hz), and the acceleration sensors were bedded in the pedestal of the faulty bearing to record the vibration signature using a sampling rate of 51.2 kHz. In this case, the BPFO of the faulty bearing is about 35.7 Hz.

Fig. 21 (a) and (b) display respectively the collected bearing vibration acceleration signature and its magnitude spectrum. The SES depicted in Fig. 21(c) cannot accurately distinguish the bearing outer race damage. Set the maximum cyclic frequency of observation to 150 Hz. It can be observed from the SCoh presented in Fig. 21(d) that the resonance frequency bands associated with bearing outer race fault are mainly located around 5 kHz and 14 kHz. In the EES shown in Fig. 21(e), the spectral line at the BPFO (marked with red dot line) can be identified, but the spectral peaks at its harmonic components are not visible.

The IESFOgram method using blind features and targeted features is utilized to deal with the same bearing vibration signature, and the obtained results (gram and IES) are demonstrated in Figs. 22 and 23, respectively. The ISFB selected by the Kurt-based method is centered at 4 kHz, while the ISFBs selected by other blind feature-based methods are around 14 kHz. The spectral line at the BPFO can be observed in the generated IESs, but the result in Fig. 22(a) is not equal to that in Fig. 22(b)-(f). It shows that the other five blind feature-based methods more accurately distinguish the resonant frequency band of bearing defect signature than the Kurt-based method. For the targeted feature-based methods, only the DF and SNR-based methods distinguish the resonance frequency bands of bearing outer race defect, with the center frequencies of 5.4 kHz and 14 kHz, respectively. The generated IESs clearly exhibit the spectral line at the BPFO, as depicted in Fig. 23(b) and (d). The other four targeted feature-based methods select a spectral frequency band centered at 800 Hz, and the resulting IESs cannot reveal the outer race defect of the tested bearing.

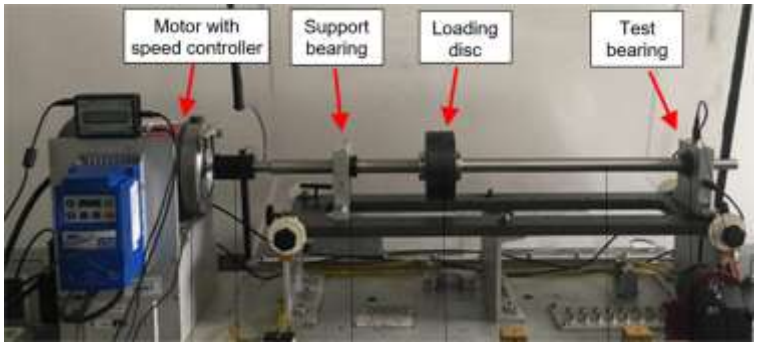

Fig. 20. UESTC bearing test rig [20].

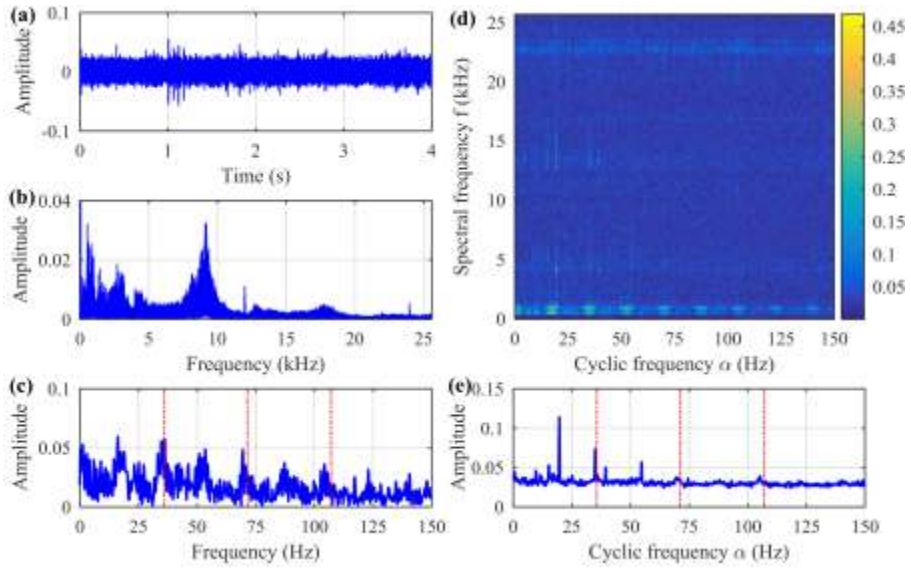

Fig. 21. Results of rolling bearing outer race defect signature: (a) signal waveform, (b) magnitude spectrum, (c) SES, (d) SCoh, and (e) EES.

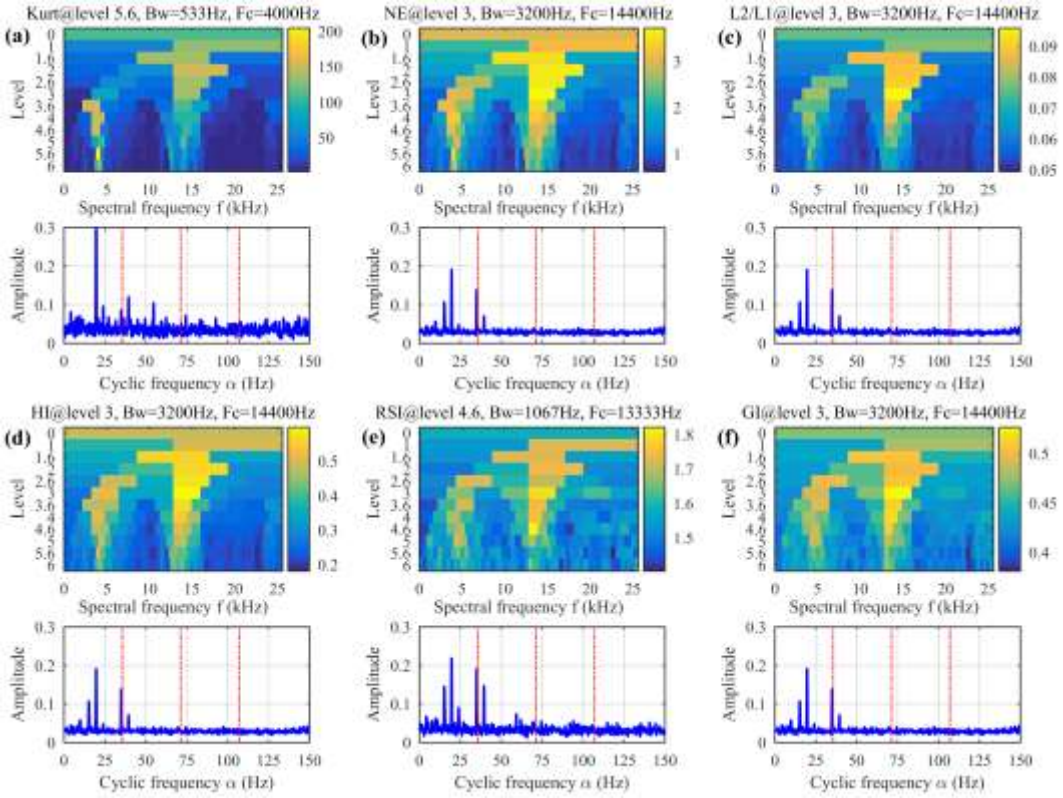

Fig. 22. Results (gram and IES) of IESFOgram based on blind features for the rolling bearing outer race defect signature: (a) Kurt, (b) NE, (c) L2/L1, (d) HI, (e) RSI, and (f) GI.

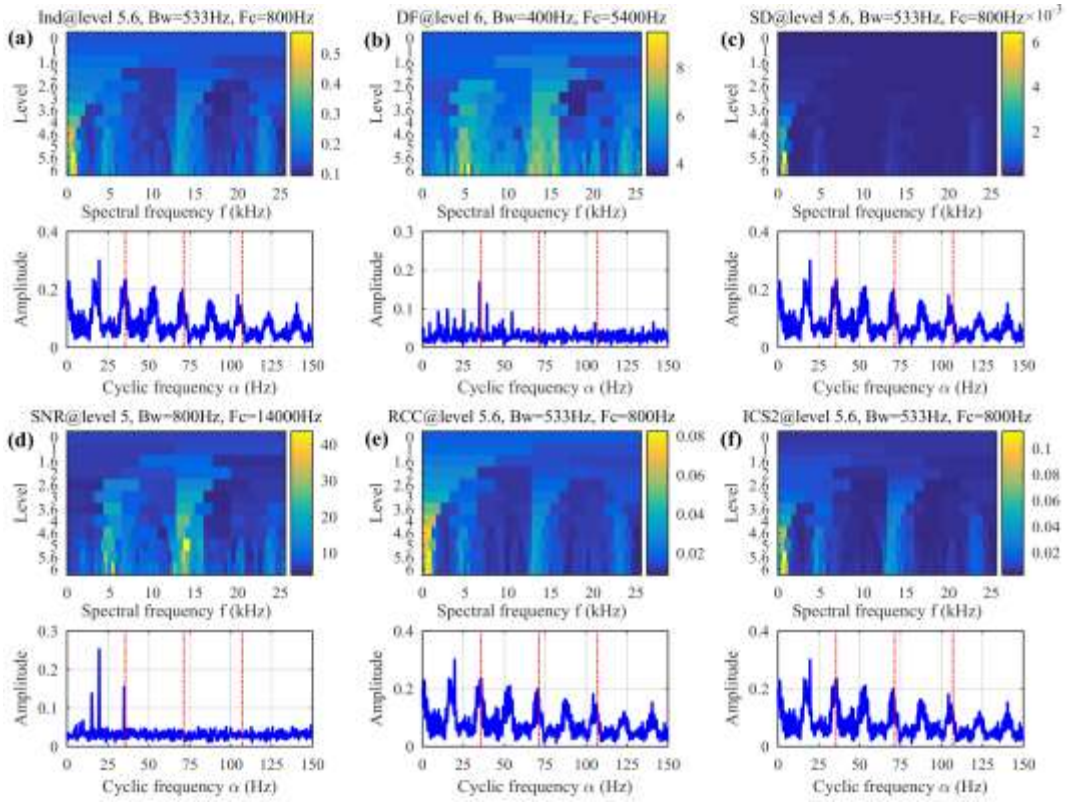

Fig. 23. Results (gram and IES) of IESFOgram based on targeted features for the rolling bearing outer race defect signature: (a) Ind, (b) DF, (c) SD, (d) SNR, (e) RCC, and (f) ICS2.

5.3. Rolling bearing inner race defect detection

The third experimental data [39] was also obtained from the UESTC bearing test rig displayed in Fig. 20. In this case, a local damage is implanted into the inner race surface of the test bearing. The sampling frequency remained unchanged, i.e., 51.2 kHz, but the spindle rotated at 3600 rpm (60 Hz). The ball pass frequency of inner race (BPFI) of the faulty bearing is 325.8 Hz.

The acquired vibration signature of the inner race defect bearing and its magnitude spectrum are respectively demonstrated in Fig. 24(a) and (b). Because of the strong disturbance noises, only the first and third harmonics of the BPFI can be discriminated in the SES exhibited in Fig. 24(c). Specify the maximum cyclic frequency of observation as 1200 Hz. The resonance frequency bands of the inner race fault bearing cannot be directly identified in the SCoh displayed in Fig. 24(d). In the EES depicted in Fig. 24(e), although the spectral peaks at the BPFI and its first two harmonic components can be discerned, they are not dominant because of the disturbance of the spectral lines at the sidebands.

Figs. 25 and 26 display the results (gram and IES) of the IESFOgram method using typical blind features and targeted features for dealing with the bearing inner race defect signature, respectively. The ISFBs selected by the blind feature-based methods are relatively wide, leading to more harmonic interferences and sidebands in the generated IESs even though the spectral lines at the fault-related frequencies can be observed, as shown in Fig. 25. The fault detection performance of the Kurt-based method is inferior to that of the other five blind feature-based methods, judging from the amplitudes at the BPFI and its harmonics in the IESs. The ISFBs selected by the targeted feature-based methods are centered around 5.8 kHz, 6.6 kHz and 7 kHz, respectively, and the spectral peaks at the BPFI and its first two harmonic components can be easily discerned in the resulting IESs, as displayed in Fig. 26.

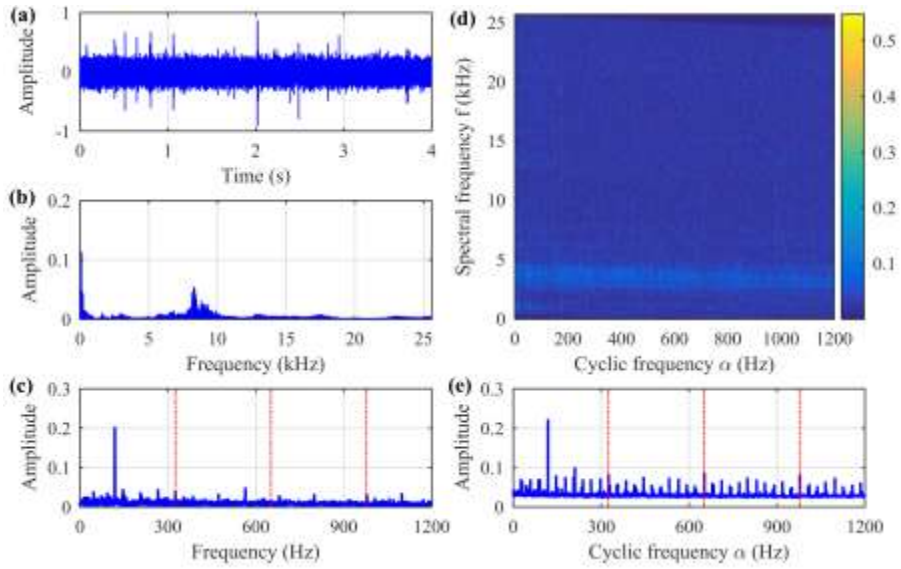

Fig. 24. Results of rolling bearing inner race defect signature: (a) signal waveform, (b) magnitude spectrum, (c) SES, (d) SCoh, and (e) EES.

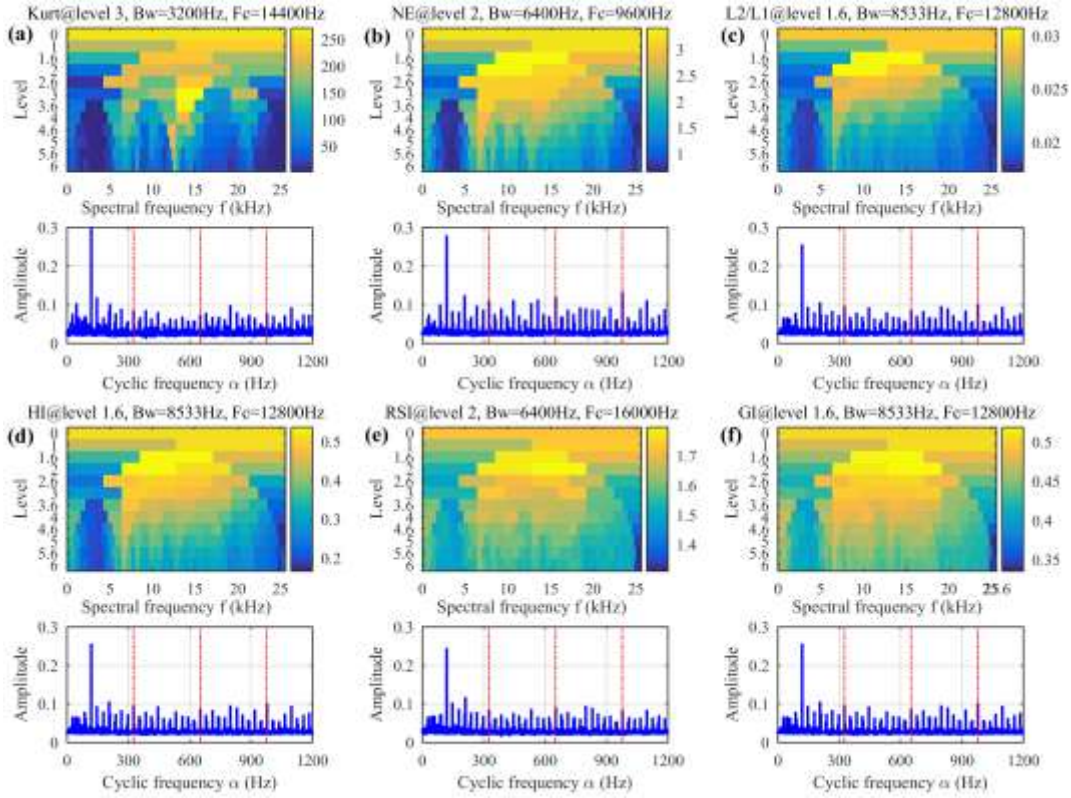

Fig. 25. Results (gram and IES) of IESFOgram based on blind features for the rolling bearing inner race defect signature: (a) Kurt, (b) NE, (c) L2/L1, (d) HI, (e) RSI, and (f) GI.

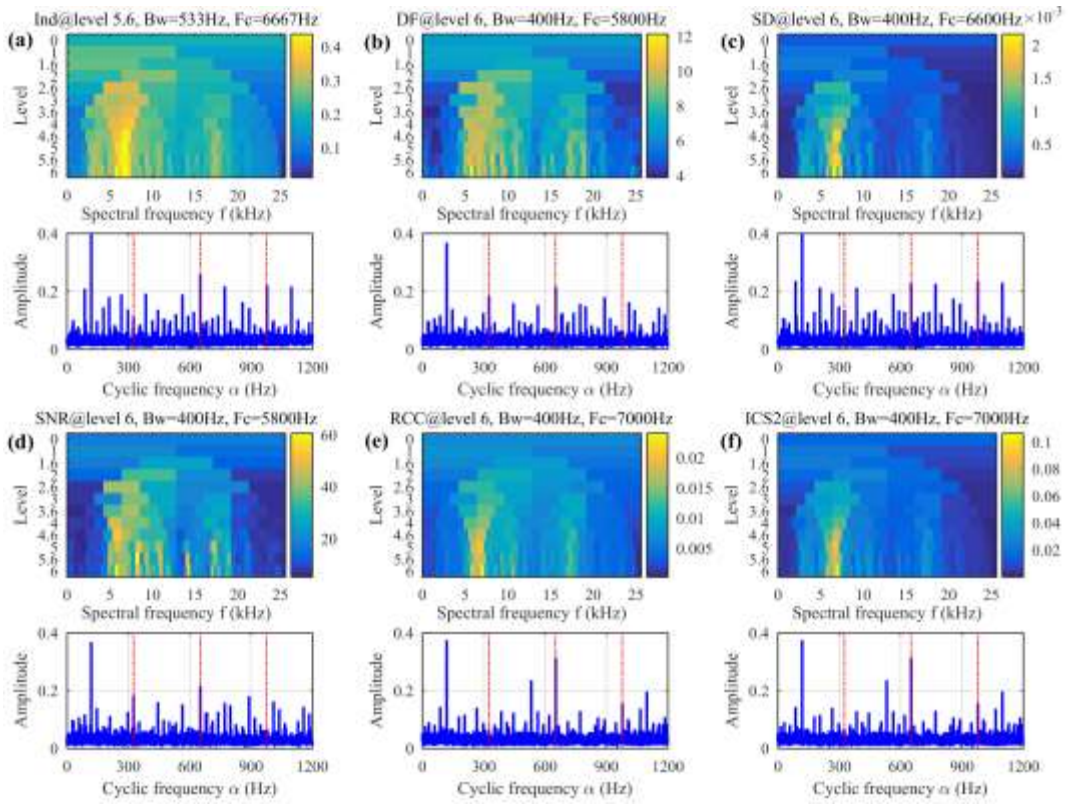

Fig. 26. Results (gram and IES) of IESFOgram based on targeted features for the rolling bearing inner race defect signature: (a) Ind, (b) DF, (c) SD, (d) SNR, (e) RCC, and (f) ICS2.

5.4. Results of proposed method on bearing experimental signals

For comparison, Fig. 27 displays the results (gram and IES) of the developed approach for processing the bearing experimental signals analyzed in the previous three subsections. Fig. 27(a) indicates that the presented approach selects the same ISFB as the SNR and RCC-based methods and effectively detects the outer race failure of the planetary bearing. When processing the rolling bearing outer race defect signal in Fig. 21(a), the proposed method selects a spectral frequency band with a bandwidth of 400 Hz and a central frequency of 13000 Hz, and the spectral lines at the BPFO and its harmonic components can be distinguished in the resulting IES, as demonstrated in Fig. 27 (b). In the experiment of bearing inner race defect detection, the spectral frequency band confirmed by the proposed method is consistent with that of the RCC and ISC2-based methods, and the inner race failure of the tested rolling bearing is demonstrated, as presented in Fig. 27(c). These experimental results prove that the presented approach effectively identifies the spectral frequency bands related to bearing faults and detects different bearing faults.

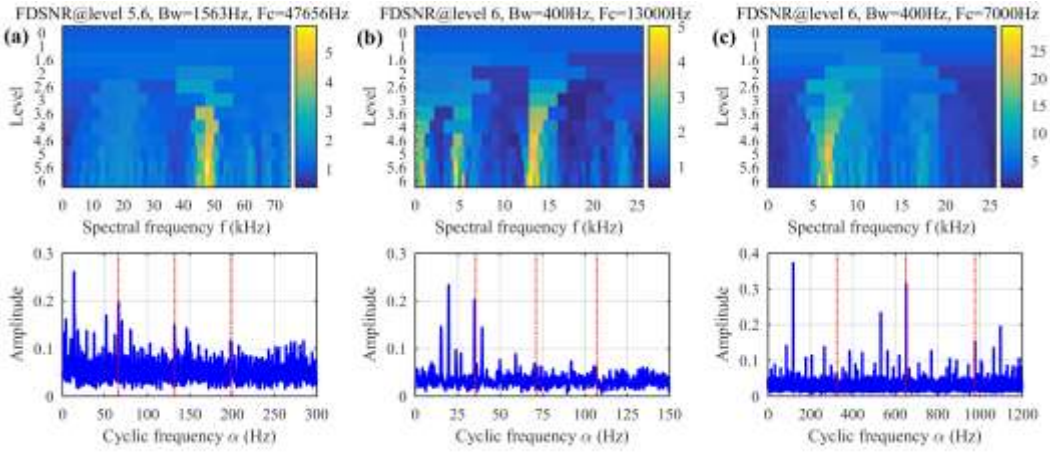

Fig. 27. Results (gram and IES) of IESFOgram based on FDSNR for different bearing experimental datasets: (a) planetary bearing outer race defect, (b) rolling bearing outer race defect, and (c) rolling bearing inner race defect.

5.5. Summary of comparison results on bearing experimental signals

The band selection and diagnosis results of IESFOgram using blind features, targeted features and FDSNR on three bearing fault cases are summarized in Table 2. The "Yes", "Partial" and "No" represent the successful diagnosis, partially successful diagnosis and unsuccessful diagnosis, respectively. Fig. 28 displays the FDSNR obtained by the blind feature-based methods, the targeted feature-based methods and the proposed method for processing three bearing experimental signals. The qualitative and quantitative results of the bearing experimental signals show that:

- The blind feature-based methods tend to select a relatively wide ISFB of the SCoh, while the targeted feature-based methods that are dedicated to disclosing the fault-related frequencies tend to construct IES over a relatively narrow ISFB.
- The Kurt-based method is susceptible to strong harmonic components in the signal. The NE-based method exhibits better performance than other blind feature-based methods in detecting different bearing faults. Therefore, the NE-based method is an alternative method when the characteristic frequency of bearing faults is unknown.
- Due to no or inappropriate normalization, the Ind, SD and ICS2-based approaches are vulnerable to high-intensity random impulse noise in the signal. Only the presented approach and the DF and SNR-based methods have detected three bearing faults, and the fault detection effect of the presented approach delivers an advantage over that of the DF and SNR-based methods. Therefore, the developed approach is preferentially recommended for bearing failure detection.

Table 2. Summary of band selection and diagnosis results of IESFOgram using different features on three bearing experimental cases.

Experiment case		Section 5.1		Section 5.2		Section 5.3	
Blind feature-based methods	Kurt	(62500,25000)	No	(4000,533)	Partial	(14400,3200)	Partial
	NE	(62500,25000)	No	(14400,3200)	Yes	(9600,6400)	Yes
	L2/L1	(62500,25000)	No	(14400,3200)	Yes	(12800,8533)	Yes
	HI	(62500,25000)	No	(14400,3200)	Yes	(12800,8533)	Yes
	RSI	(3125,6250)	No	(13333,1067)	Yes	(16000,6400)	Yes
	GI	(6250,12500)	No	(14400,3200)	Yes	(12800,8533)	Yes
Targeted	Ind	(15820,1172)	No	(800,533)	No	(6667,533)	Yes

feature-based	DF	(45117,1172)	Yes	(5400,400)	Yes	(5800,400)	Yes
methods	SD	(15820,1172)	No	(800,533)	No	(6600,400)	Yes
	SNR	(47656,1563)	Yes	(14000,800)	Yes	(5800,400)	Yes
	RCC	(47656,1563)	Yes	(800,533)	No	(7000,400)	Yes
	ICS2	(15820,1172)	No	(800,533)	No	(7000,400)	Yes
	FDSNR	(47656,1563)	Yes	(13000,400)	Yes	(7000,400)	Yes

Note: (CF, BW) denotes the selected ISFB, CF = center frequency (Hz) and BW = bandwidth (Hz).

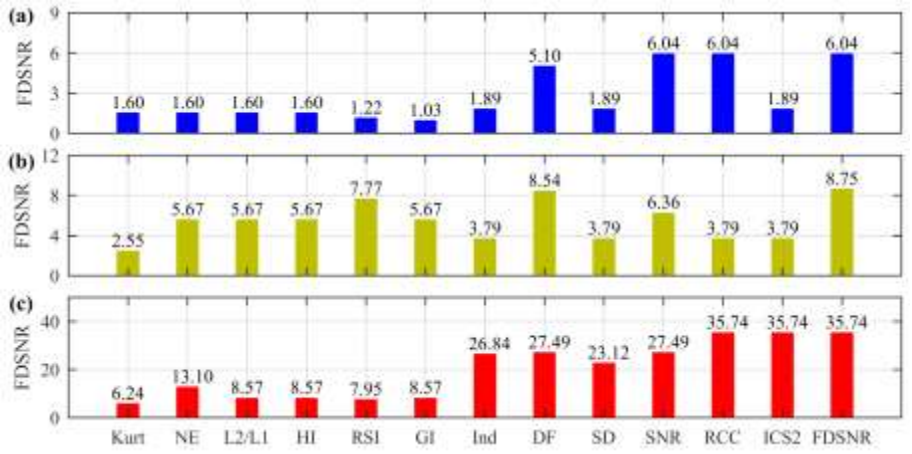

Fig. 28. FDSNR obtained by IESFOgram using different features for different bearing experimental datasets: (a) planetary bearing outer race defect, (b) rolling bearing outer race defect, and (c) rolling bearing inner race defect.

6. Conclusions

In this article, a novel targeted feature is presented to evaluate bearing failure information in the cyclic frequency domain, and a novel method based on the proposed feature is developed to distinguish an optimal spectral frequency band of spectral coherence for constructing diagnostic improved envelope spectrum. The efficiency of the developed approach is testified using the simulated and experimental signals, and is compared with the typical blind feature-based methods and targeted feature-based methods. The results indicate the following conclusions:

(1) The blind feature-based methods have certain resistance to Gaussian white noise and random impulse noise but are susceptible to impulsive cyclostationary noise and discrete harmonics. The negentropy-based method exhibits better performance than other blind feature-based methods in detecting different bearing faults and therefore it can be regarded as an alternative method when the fault characteristic frequency is unknown.

(2) The band selection accuracy and fault detection ability of the presented approach and the diagnostic feature and signal-to-noise ratio-based methods are superior to that of the blind feature-based methods and other targeted feature-based methods under the presence of Gaussian noise and typical non-Gaussian noises, especially the proposed approach. Hence, the developed approach is preferentially recommended for bearing failure detection.

In further research, the proposed method can be employed to fault diagnosis of other rotating machinery and variable speed conditions, and the proposed feature can be applied to fault information evaluation in other diagnosis methods. On the other hand, since the developed approach requires the interested fault characteristic frequency as an input parameter, the development of a feature indicator that is less dependent on fault knowledge and robust to interference noises is also part of further work.

References

[1] Randall RB, Antoni J. Rolling element bearing diagnostics-A tutorial. Mech Syst Signal Process 2011;25:485–520.

[2] Soualhi A, Medjaher K, Zerhouni N. Bearing health monitoring based on Hilbert-Huang transform, support vector machine, and regression. IEEE Trans Instrum Meas 2015;64:52–62.

[3] Zhang C, Liu Y, Wan F, Chen B, Liu J, Hu B. Adaptive filtering enhanced windowed correlated kurtosis for multiple faults diagnosis of locomotive bearings. ISA Trans 2020;101:421–9.

[4] Albezzawy MN, Nassef MG, Sawalhi N. Rolling element bearing fault identification using a novel three-step adaptive and automated filtration scheme based on Gini index. ISA Trans 2020;101:453–60.

[5] Antoni J. Fast computation of the kurtogram for the detection of transient faults. Mech Syst Signal Process 2007;21:108–24.

[6] Barszcz T, Jabłoński A. A novel method for the optimal band selection for vibration signal demodulation and comparison with the Kurtogram. Mech Syst Signal Process 2011;25:431–51.

[7] Antoni J. The infogram: Entropic evidence of the signature of repetitive transients. Mech Syst Signal Process 2016;74:73–94.

[8] Tse PW, Wang D. The design of a new sparsogram for fast bearing fault diagnosis: Part 1 of the two related manuscripts that have a joint title as “two automatic vibration-based fault diagnostic methods using the novel sparsity measurement - Parts 1 and 2.” Mech Syst Signal Process 2013;40:499–519.

[9] Hoyer PO. Non-negative matrix factorization with sparseness constraints. J Mach Learn Res 2004;5:1457–69.

[10] Bozchalooi IS, Liang M. A smoothness index-guided approach to wavelet parameter selection in signal de-noising and fault detection. J Sound Vib 2007;308:246–67.

[11] Miao Y, Zhao M, Lin J. Improvement of kurtosis-guided-grams via Gini index for bearing fault feature identification. Meas Sci Technol 2017;28:125001.

[12] Hebda-Sobkowicz J, Zimroz R, Pitera M, Wyłomańska A. Informative frequency band selection in the presence of non-Gaussian noise – a novel approach based on the conditional variance statistic with application to bearing fault diagnosis. Mech Syst Signal Process 2020;145:106971.

[13] Wang D. Some further thoughts about spectral kurtosis, spectral L2/L1 norm, spectral smoothness index and spectral Gini index for characterizing repetitive transients. Mech Syst Signal Process 2018;108:58–72.

[14] Miao Y, Zhao M, Hua J. Research on sparsity indexes for fault diagnosis of rotating machinery. Measurement 2020;158:107733.

[15] Hebda-Sobkowicz J, Zimroz R, Wyłomanska A. Selection of the informative frequency band in a bearing fault diagnosis in the presence of non-gaussian noise-Comparison of recently developed methods. Appl Sci 2020;10:2657.

[16] Smith WA, Randall RB, du Mée X de C, Peng P. Use of cyclostationary properties to diagnose planet bearing faults in variable speed conditions. 10th DST Gr Int Conf Heal Usage Monit Syst 17th Aust Aerosp Congr 2017:26–8.

[17] Borghesani P, Pennacchi P, Chatterton S. The relationship between kurtosis- and envelope-based indexes for the diagnostic of rolling element bearings. Mech Syst Signal

Process 2014;43:25–43.

[18] Luo C, Mo Z, Miao Q. Cyclic harmonic ratio defined in squared envelope spectrum and log-envelope spectrum for gearbox fault diagnosis. IEEE Trans Instrum Meas 2020;69:9568–77.

[19] Ni Q, Wang K, Zheng J. Rolling element bearings fault diagnosis based on a novel optimal frequency band selection scheme. IEEE Access 2019;7:80748–66.

[20] Smith WA, Borghesani P, Ni Q, Wang K, Peng Z. Optimal demodulation-band selection for envelope-based diagnostics: A comparative study of traditional and novel tools. Mech Syst Signal Process 2019;134:106303.

[21] Randall RB, Antoni J, Chobsaard S. The relationship between spectral correlation and envelope analysis in the diagnostics of bearing faults and other cyclostationary machine signals. Mech Syst Signal Process 2001;15:945–62.

[22] Antoni J. Cyclic spectral analysis of rolling-element bearing signals: Facts and fictions. J Sound Vib 2007;304:497–529.

[23] Antoni J, Xin G, Hamzaoui N. Fast computation of the spectral correlation. Mech Syst Signal Process 2017;92:248–77.

[24] Wang D, Zhao X, Kou LL, Qin Y, Zhao Y, Tsui KL. A simple and fast guideline for generating enhanced/squared envelope spectra from spectral coherence for bearing fault diagnosis. Mech Syst Signal Process 2019;122:754–68.

[25] Xiao C, Tang H, Ren Y, Xiang J, Kumar A. A fault frequency bands location method based on improved fast spectral correlation to extract fault features in axial piston pump bearings. Measurement 2021;171:108734.

[26] Mauricio A, Qi J, Smith WA, Sarazin M, Randall RB, Janssens K, et al. Bearing diagnostics under strong electromagnetic interference based on Integrated Spectral Coherence. Mech Syst Signal Process 2020;140:106673.

[27] Mauricio A, Smith WA, Randall RB, Antoni J, Gryllias K. Improved Envelope Spectrum via Feature Optimisation-gram (IESFOgram): A novel tool for rolling element bearing diagnostics under non-stationary operating conditions. Mech Syst Signal Process 2020;144:106891.

[28] Mauricio A, Qi J, Gryllias K. Vibration-based condition monitoring of wind turbine gearboxes based on cyclostationary analysis. J Eng Gas Turbines Power 2019;141:1–8.

[29] Mauricio A, Sheng S, Gryllias K. Condition monitoring of wind turbine planetary gearboxes under different operating conditions. J Eng Gas Turbines Power 2020;142:1–8.

[30] Mauricio A, Qi J, Zhou L, Wang W, Mba D, Gryllias K. Perspectives on Health and Usage Monitoring Systems (HUMS) of helicopters. MATEC Web Conf 2020;314:02008.

[31] Mauricio A, Zhou L, Mba D, Gryllias K. Vibration based condition monitoring of helicopter gearboxes based on cyclostationary analysis. Proc ASME Turbo Expo 2019;6:1–7.

[32] Mauricio A, Gryllias K. Cyclostationary-based Multiband Envelope Spectra Extraction for bearing diagnostics: The Combined Improved Envelope Spectrum. Mech Syst Signal Process 2021;149:107150.

[33] Schmidt S, Mauricio A, Heyns PS, Gryllias KC. A methodology for identifying information rich frequency bands for diagnostics of mechanical components-of-interest under time-varying operating conditions. Mech Syst Signal Process 2020;142:106739.

[34] Antoni J. Cyclic spectral analysis in practice. Mech Syst Signal Process 2007;21:597–630.

[35] Antoni J, Hanson D. Detection of surface ships from interception of cyclostationary signature

with the cyclic modulation coherence. IEEE J Ocean Eng 2012;37:478–93.

[36] Borghesani P, Antoni J. A faster algorithm for the calculation of the fast spectral correlation. Mech Syst Signal Process 2018;111:113–8.

[37] Smith W, Borghesani P, Ni Q, Wang K, Peng Z. Data5-1_Test1_ConstSpeed10sec_section.mat (https://www.researchgate.net/publication/337067239_Data5-1_Test1_ConstSpeed10sec_sectionmat) 2019.

[38] Smith W, Borghesani P, Ni Q, Wang K, Peng Z. Data5-2_10Hz-outer3.mat (https://www.researchgate.net/publication/337067356_Data5-2_10Hz-outer3mat) 2019.

[39] Smith W, Borghesani P, Ni Q, Wang K, Peng Z. Data5-3_60Hz-inner.mat (https://www.researchgate.net/publication/337067159_Data5-3_60Hz-innermat) 2019.